Toward Designed Singlet Fission: Electronic States and Photophysics of 1,3-Diphenylisobenzofuran

ARTICLE *in* THE JOURNAL OF PHYSICAL CHEMISTRY A · DECEMBER 2009

Impact Factor: 2.69 · DOI: 10.1021/jp907401t · Source: PubMed

Toward Designed Singlet Fission: Electronic States and Photophysics of 1,3-Diphenylisobenzofuran†

Andrew F. Schwerin,‡ Justin C. Johnson,§ Millicent B. Smith,‡ Paiboon Sreearunothai,|| Duška Popović,‡ Jiří Černý,⊥ Zdeněk Havlas,⊥ Irina Paci,# Akin Akdag,‡ Matthew K. MacLeod,‡ Xudong Chen,‡ Donald E. David,‡ Mark A. Ratner,# John R. Miller,|| Arthur J. Nozik,§ and Josef Michl*,‡,⊥

Department of Chemistry and Biochemistry, University of Colorado, 215 UCB, Boulder, Colorado 80309-0215, National Renewable Energy Laboratory, 1617 Cole Blvd., Golden, Colorado 80401-3393, Brookhaven National Laboratory, 2 Center Street, Upton, New York 11973, Institute of Organic Chemistry and Biochemistry, Academy of Sciences of the Czech Republic, Flemingovo n. 2, 166 10 Prague 6, Czech Republic, and Department of Chemistry, Northwestern University, 2145 Sheridan Road, Evanston, Illinois 60208-3113

Received: July 31, 2009; Revised Manuscript Received: November 6, 2009

Single crystal molecular structure and solution photophysical properties are reported for 1,3-diphenylisobenzofuran (**1**), of interest as a model compound in studies of singlet fission. For the ground state of **1** and of its radical cation ($\mathbf{1}^{+\bullet}$) and anion ($\mathbf{1}^{-\bullet}$), we report the UV−visible absorption spectra, and for neutral **1**, also the magnetic circular dichroism (MCD) and the decomposition of the absorption spectrum into purely polarized components, deduced from fluorescence polarization. These results were used to identify a series of singlet excited states. For the first excited singlet and triplet states of **1**, the transient visible absorption spectra, $S_1 \rightarrow S_x$ and sensitized $T_1 \rightarrow T_x$, and single exponential lifetimes, $\tau_F = \sim 5.3$ ns and $\tau_T = \sim 200\ \mu$s, are reported. The spectra and lifetimes of $S_1 \rightarrow S_0$ fluorescence and sensitized $T_1 \rightarrow T_x$ absorption of **1** were obtained in a series of solvents, as was the fluorescence quantum yield, $\Phi_F = 0.95-0.99$. No phosphorescence has been detected. The first triplet excitation energy of solid **1** (11 400 cm^{-1}) was obtained by electron energy loss spectroscopy, in agreement with previously reported solution values. The fluorescence excitation spectrum suggests an onset of a nonradiative channel at ∼37 000 cm^{-1}. Excitation energies and relative transition intensities are in agreement with those of ab initio (CC2) calculations after an empirical 3000 cm^{-1} adjustment of the initial state energy to correct differentially for a better quality description of the initial relative to the terminal state of an absorption transition. The interpretation of the MCD spectrum used the semiempirical PPP method, whose results for the $S_0 \rightarrow S_x$ spectrum require no empirical adjustment and are otherwise nearly identical with the CC2 results in all respects including the detailed nature of the electronic excitation. The ground state geometry of **1** was also calculated by the MP2, B3LYP, and CAS methods. The calculations provided a prediction of changes of molecular geometry upon excitation or ionization and permitted an interpretation of the spectra in terms of molecular orbitals involved. Computations suggest that **1** can exist as two nearly isoenergetic conformers of C_2 or C_s symmetry. Linear dichroism measurements in stretched polyethylene provide evidence for their existence and show that they orient to different degrees, permitting a separation of their spectra in the region of the purely polarized first absorption band. Their excitation energies are nearly identical, but the Franck−Condon envelopes of their first transition differ to a surprising degree.

Introduction

Why Singlet Fission? One of the factors limiting the efficiency of conventional single-stage solar cells having a single light-absorbing phase is that part of the energy of photons absorbed above the threshold energy (bandgap) is converted into heat and only the energy that corresponds to the lowest energy transition of the absorbing medium is available to produce useful free energy in the form of photopotential. One of the ways in which the photons of the high-energy end of the solar spectrum might be better utilized is to take advantage of singlet fission.[1−4] In this process,[5,6] an excited singlet state of a chromophore, such as that initially generated by photon absorption, shares its energy $E(S_1)$ with a nearby chromophore, producing a triplet excited state of each at energy $E(T_1)$.

If both triplet excitations generated by singlet fission had sufficient energy for electron−hole pair production and were coupled weakly enough to act independently, the photocurrent per photon would be doubled. Those photons whose energy is below $E(S_1)$ but above $E(T_1)$ would be absorbed by a subsequent layer of an ordinary sensitizer chosen to have its absorption edge at $\sim E(T_1)$ and capable of yielding a single electron−hole pair per photon (Figure 1). Given the spectral distribution of the solar flux at the surface of the earth, this scheme offers a maximum efficiency of ∼46%,[7] significantly higher than the ordinary Shockley−Queisser limit of ∼32%.[8] Optimal theoretical performance is attained near $E(S_1) = \sim 2.2$ eV and $E(T_1) = \sim 1.1$ eV. There is an additional advantage to the use of triplets for charge injection, as back electron transfer to yield the ground

† Part of the "W. Carl Lineberger Festschrift".
‡ University of Colorado.
§ National Renewable Energy Laboratory.
|| Brookhaven National Laboratory.
⊥ Academy of Sciences of the Czech Republic.
Northwestern University.

10.1021/jp907401t
Published on Web 12/21/2009

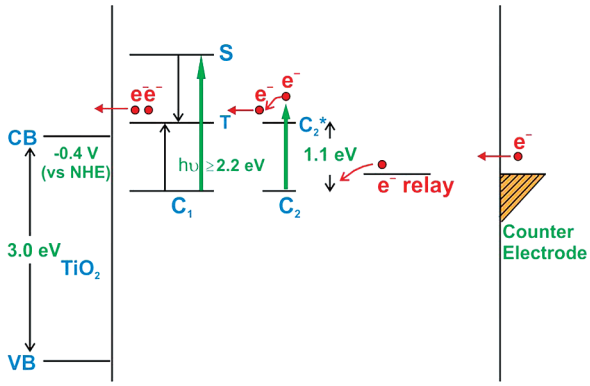

Figure 1. Processes occurring in a singlet fission solar cell (schematic).

state is spin-forbidden. Triplets also offer much longer excited state lifetimes, providing more opportunity for injection. These advantages may be partly negated by increased opportunities for quenching by the hole-transporting shuttle such as the iodide ion, and by the generally lower triplet mobility.

Parallel efforts are underway with quantum dots, in which more than one exciton can apparently be generated by the absorption of a single photon.[9−12] They are more likely to be light-stable and offer the advantage that the formation of more than two electron−hole pairs from a single photon seems to already have been observed. Their primary disadvantage is the very short lifetime of the multiple excitons produced.

Present Status. Little is known about conditions under which singlet fission in a sensitizer adsorbed on a semiconductor such as nanocrystalline TiO_2 might be efficient. It has been observed on a series of more or less randomly chosen crystalline, polymeric, and oligomeric chromophores that all happen to be alternant hydrocarbons or their simple derivatives. Numerous references to this work were collected in 2006[4] and will not be repeated here. Recently, singlet fission in covalent dimers has been investigated as well.[13−15] Although the quantum yields with which triplets were formed were believed to be high in some instances, little or no effort has gone into their actual direct measurement. Values reported for covalent dimers so far were on the order of a few percent. Only values substantially above 100% offer any prospect to make the approach worthwhile, and the theoretical efficiency quoted above is based on an assumption of a 200% triplet yield.

Can one go from a few percent to 200%? Two obvious initial steps are:

(i) Identification of suitable monomeric chromophores. In these, all processes capable of depopulating the singlet state that is to undergo fission need to have a negligible rate. Specifically, they are vibrational deactivation, internal conversion, intersystem crossing, fluorescence, and photoinduced electron transfer producing charge separation (i.e., free charge carriers). Also, conditions for the reverse process, triplet−triplet annihilation, should be unfavorable.

(ii) Determination of the degree of interchromophore coupling that is necessary for fast singlet fission in a dimer or higher aggregate and yet permits the two resulting triplets to behave independently enough for each to generate free charge carriers through charge transfer.

In the present series of papers, we only address these two fundamental problems. Once general answers to them are known, it will be appropriate to consider addressing others, such as an optimization of the energy of the absorption edge and of the molecular energy levels relative to those of the electron or hole injection partners, stabilizing the sensitizer under irradiation, and coupling it properly to the injection partner, such that the short-lived initially produced singlet does not form free charge carriers prematurely, but the subsequently formed, longer lived triplets do so efficiently.

Initial Steps. ***(i) Chromophore Choice.*** The singlet fission process is spin-allowed and can be very fast. It has been observed to compete significantly with vibrational deactivation in the crystalline shorter polyacenes, where it only occurs from vibrationally hot S_1 or from higher singlets, since the vibrationally relaxed S_1 state does not have enough energy to produce two T_1 states. All concerns about fast vibrational relaxation will be eliminated if we choose a chromophore in which $E(S_1) \geq 2E(T_1)$ holds for the relaxed S_1 state.

The remaining concerns will be addressed automatically if we only work with strongly fluorescent chromophores. The fluorescence rate constant will rarely exceed 10^9 s^{-1}, and a high fluorescence quantum yield will guarantee that all other competing processes in the monomer are even slower. It will then be sufficient for the rate constant of singlet fission in the dimer to exceed $10^{10}-10^{11}$ s^{-1} to outcompete fluorescence, as long as no additional competitive processes such as charge separation take place in the dimer, oligomer, aggregate, or crystal.

Preventing triplet−triplet annihilation in the dimer is another important consideration. Recombination to yield $S_0 + S_0$ or $S_0 + T_1$ is likely to be highly exothermic, in the inverted region and slow, while annihilation to yield $S_0 + S_1$ or $S_0 + Q_1$ (quintet) will be endothermic and also slow. However, fast annihilation to yield $S_0 + T_2$ could be a problem if $E(T_2)$ lies a little below $2E(T_1)$. The best pair of conditions to impose therefore seems to be $E(S_1)$, $E(T_2) \geq 2E(T_1)$, which will ensure that both the annihilation path that yields $S_0 + S_1$ and the one that yields $S_0 + T_2$ are endothermic and slow. These were the conditions imposed in our preceding paper, which addressed the issue of rational guidelines for the design of monomeric chromophores for efficient singlet fission.[4]

(ii) Chromophore Coupling. In the third paper of the series,[16] we present the results of an extensive computational examination of the degree of coupling that can be achieved by the various ways in which selected chromophores can be coupled into dimers. Elsewhere,[17] the possible role of charge-transfer states in singlet fission is examined theoretically. The fourth,[18] fifth,[18] and sixth[19] papers describe our initial experimental efforts to identify a suitable degree of coupling of the monomeric chromophore **1** that would optimize conditions for singlet fission. The fourth paper is devoted to weakly coupled covalent dimers of **1**, for which we have found interesting photophysics with some evidence for singlet fission. The fifth paper deals with a strongly coupled dimer, for which a singlet fission triplet yield of a few % has been observed. The sixth one deals with the use of films of neat solid **1**, for which we have estimated triplet yields exceeding 100%, depending significantly on the details of film preparation. This is remarkable, since the latest estimates of the yield of triplets formed by singlet fission in evaporated films of pentacene, which also satisfies the condition $E(S_1)$, $E(T_2) \geq 2E(T_1)$, are less than 10%, with charge separation representing the main competing pathway.[20] The yields are much higher and possibly quantitative in a pentacene single crystal, where singlet fission occurs on a subps time scale, but they have not been measured directly.[21] We suspect that the striking dependence of the properties of the films of **1** on deposition conditions is related to the existence of two conformers of **1**, and therefore pay attention to this issue in the present paper.

A preliminary account of some of our experimental results has appeared.[15]

1,3-Diphenylisobenzofuran (1). Our initial paper[4] suggested two classes of structures as particularly promising for the monomeric chromophores. Both are of the conjugated π-electron type, which is likely to offer high absorption coefficients, needed at all wavelengths shorter than the absorption threshold. The parent structures for the two classes are alternant hydrocarbons and biradicaloids, respectively. Numerical computations identified several types of chromophores that belong to both classes simultaneously as worthy of further investigation, and we have chosen the monomer **1** as a particularly suitable model for an initial examination,[15] since it is strongly fluorescent, suggesting the absence of significant dark channels depopulating the S_1 state, and its known[22] values $E(S_1) = \sim 24\,300$ (vertical) and $E(T_1) = 11\,900 \pm 100$ (adiabatic) cm^{-1} meet the condition $E(S_1) \geq 2E(T_1)$. Calculations[4] suggested that the condition $E(T_2) \simeq 2E(T_1)$ is satisfied as well. Monomeric **1** is available commercially, and the synthesis of various dimers and oligomers appeared quite feasible. Nevertheless, **1** is not an ideal model, since its $E(S_1)$ and $E(T_1)$ energies are considerably higher than the optimal $\sim 17\,600$ and ~ 8800 cm^{-1}, respectively, and the instability of the parent to irradiation in the presence of air suggests that its derivatives have little chance of being practically useful.

Unlike the spectra and photophysics of many of the chromophores that were chosen for singlet fission studies in the past, those of **1** were not understood in detail, even though it has seen considerable use for semiquantitative detection of singlet oxygen through the monitoring of its intense first UV absorption band,[23] and its T_1 energy was determined by sensitization[22] and from electroluminescence.[24] We have started our investigations of singlet fission in the covalent dimers and crystals of **1** by performing a thorough characterization of its electronic states and photophysics in the expectation that it will be needed for the study of the photophysics of its dimers and higher aggregates, and report the results here.

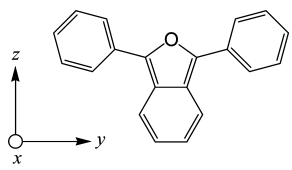

1

Experimental Part and Calculations

Materials. Commercial anthracene (Aldrich, 99%) was used. Commercial **1** (Aldrich) had identical properties as received and after purification by gradient sublimation. No impurities were detected by NMR. It was stored and solutions were prepared and handled under an oxygen and water-free helium atmosphere in a glovebox. Solvents (dimethyl sulfoxide, DMSO; acetonitrile, AN; tetrahydrofuran, THF; cyclohexane, CH; toluene, TOL; *N*,*N*-dimethylformamide, DMF; and 1,2-dichloroethane, DCE) were purchased from Aldrich (highest purity) and were used as received. 3-Methylpentane, 3-MP, was purchased from Chevron Phillips and purified as described by Murray and Keller.[25] The solvents were flushed with argon for at least 30 min before transfer to the glovebox. Sample cells were sealed in the glovebox before being taken into ambient conditions for use. Although **1** is photolabile in the presence of oxygen,[23] solutions prepared under these conditions showed only very minor signs of degradation after many hours of CW (20 mW/cm^2) or pulsed (1 mJ/cm^2, 5 ns pulse) irradiation. Under more intense pulsed irradiation, however, significant degradation occurred in minutes.

Temperature Control in Spectroscopy. Unless stated otherwise, temperatures between 77 and 500 K were maintained using an Oxford Instruments liquid nitrogen cryostat modified for holding a 1 cm (steady state and flash photolysis measurements) or 2 mm (femtosecond transient absorption measurements) quartz cell.

Absorption Spectra. Room temperature and low-temperature UV−vis absorption spectra of $\sim 10^{-5}$ M solutions in 3-MP were recorded in a Suprasil quartz cell with 1 cm path length using a Shimadzu 3600 UV/vis/NIR or a HP 8452A diode array spectrophotometer. Oscillator strengths f were calculated from $f = 4.319 \times 10^{-9} \int d\tilde{\nu}\, \varepsilon(\tilde{\nu})$.[26a]

Linear Dichroism (LD). The UV−vis LD spectra of **1** absorbed into a stretched polyethylene sheet were obtained with a JASCO J-720 spectropolarimeter operating in LD mode. Polyethylene sheets were cut from a commercial polyethylene bag and cleaned twice by soaking in chloroform overnight with stirring, rinsing with methylene chloride and drying. The purified sheets were stretched to approximately five times their original length. A few drops of a saturated solution of the sample in chloroform were added to one face of the stretched sheet in a covered dish containing a small amount of chloroform. After 1 h, the saturated solution was allowed to evaporate from the sheet, and any crystals remaining on the surface of the sheet were removed by gentle wiping with lens tissue, followed by rinsing with methanol. The stretched sheet was positioned in the spectrometer such that the photoelastic modulator produced light that alternated between polarizations parallel and perpendicular to the stretching direction. A baseline was obtained by recording the spectrum after most of the solute had been washed out of the sheet with chloroform.

Magnetic Circular Dichroism (MCD). MCD spectra in cyclohexane were run in a 1 cm Suprasil quartz cell using a JASCO J-720 spectropolarimeter fitted with a 1.504 T electromagnet. The magnetic field was parallel to the direction of light propagation, and 12 spectra run at a resolution of 2 nm, a speed of 50 nm/min, a response time of 1 s, a bandwidth of 1.0 nm, and a sensitivity of 5 mdeg were averaged for each sample. B terms were calculated from $B = -2.98 \times 10^{-2} \int d\tilde{\nu}\, [\Theta(\tilde{\nu})]_M/\tilde{\nu}$.[26b]

Steady State Fluorescence. Corrected room-temperature fluorescence spectra and quantum yields Φ_F were obtained at 90° excitation using a Photon Technologies International Quantamaster spectrometer, with Rhodamine 6G in ethanol ($\Phi_F = 0.94$) as standard.[27] Φ_F values were corrected for solvent refractive index difference.[28] The solutions had equal absorbance at the excitation wavelength, chosen to be less than 0.1.

Fluorescence Polarization. These measurements used a spectrofluorometer consisting of a Spex double 0.5 m excitation monochromator (model 1302) with two ruled gratings (1200 grooves per mm) and a Spex 0.75 m emission monochromator (model 1702) with a holographic grating (1200 grooves per mm) assembled in a front-face configuration. CW illumination was provided by a 300 W Xe arc lamp. Glan−Taylor polarizers were placed between the sample and each monochromator, and fluorescence spectra were taken with polarizers aligned in four combinations (∥/∥), (∥/⊥), (⊥,∥), and (⊥,⊥). A depolarizing prism was placed in front of the emission monochromator to avoid bias in emission collection and detection toward one polarization over the other. The measurements were made in a 3-MP glass produced by cooling the sample to 77 K in a liquid nitrogen filled quartz dewar with Suprasil windows. Sample solutions

were kept in stemmed Suprasil quartz cells with stopcocks and degassed using several freeze−pump−thaw cycles. Standard procedures[26c] were used to convert the four polarized fluorescence spectra into the fluorescence anisotropy curve. The maximum and minimum values of anisotropy were +0.38 and −0.17, respectively, and the difference to the ideal values of +0.4 and −0.2 was attributed to accidental depolarization. A correction for this error was introduced by multiplying the anisotropy curve with a factor of 1.114, which brought the average value in the region of the first absorption band to coincidence with the 0.4 value expected for a purely polarized first transition.

Fluorescence Decay. Fluorescence decay was measured with a time-correlated single photon counting apparatus, using a frequency-doubled pulsed Ti:sapphire oscillator (Spectra-Physics Tsunami, $\lambda = 405$ nm, 80 MHz, 200 fs pulse width), modulated at 200 kHz. Including the multichannel plate detector response time, a 50 ps instrument resolution was achieved.

Transient Absorption. Ultrafast pump−probe experiments were performed using an amplified Ti:sapphire laser (Clark CPA-2001, 775 nm, 1 kHz, 0.6 mJ/pulse). The excitation was provided by frequency doubling the fundamental beam, with the probe continuum (450−700 nm) generated by focusing 1 mW of the fundamental beam into a sapphire plate. The probe beam was delayed up to 8 ns via multiple passes off a delay stage before being split into two parallel paths and focused (200 μm waist) into the sample. The excitation beam was modulated at 500 Hz, focused to 0.5 mm at the sample position, and spatially overlapped with one probe beam. Probe beams were directed to a monochromator with a dual Si photodiode detector at the exit. Signals were directed to a lock-in amplifier, and the differential transmittance at each time delay and wavelength was calculated. After correction for the chirp of the continuum, instrumental time resolution was limited by the pump pulse duration (150 fs). Flash photolysis was performed using a beam from a tunable OPO pumped by a tripled Nd:YAG laser (Continuum, Surelite II, 10 Hz, 5 ns pulse) as the excitation, and a broadband pulsed Xe arc lamp as the probe. The pump pulse energy was typically 0.5−5 mJ, and the beam was directed unfocused (about 1 cm waist) into the sample solution. The output of the lamp was masked and directed into the sample (about 3 mm waist) orthogonal to the pump beam. A 1 cm path length cell with the sample solution was placed at the intersection of the pump and probe beams. Differential absorbance was calculated from the normalized difference in transmitted probe intensity before and after arrival of the pump pulse.

Global Fitting. Traces of normalized differential absorbance ($\Delta\alpha/\alpha$) vs time delay at various probing wavelengths were fitted globally to produce ground state bleach, stimulated emission, and excited state absorption spectra. Ground state bleach and stimulated emission components were constrained to be identical in shape to the steady-state UV-VIS absorption and fluorescence spectra, respectively, allowing the identification of the purely absorptive S1-Sx features.

Electron Energy Loss Spectroscopy (EELS). The measurements were done using a high-resolution LK 2000 EEL spectrometer. It was modified for position-sensitive detection by use of a microchannel plate.[29] The spectrometer is located in UHV system with a base pressure of 1×10^{-10} Torr and a minimum pressure of 8×10^{-12} Torr, when the cryostat is cooled with liquid He. A monolayer (ML) of **1** was deposited onto a Ag(111) crystal substrate mounted at the end of the cryostat by condensing a vapor obtained by heating the sample cell containing **1** to 80 °C and holding it close to the Ag(111) crystal kept at a liquid nitrogen or helium temperature. The film thickness was calibrated to an accuracy of ±10% with a quartz microbalance mounted on the sample holder next to the crystal. The combined resolution of the two energy selectors (monochromator and analyzer) was between 12 and 20 meV full width at half-maximum (fwhm). The spectrum presented here was acquired at an incident electron energy of 2.5 eV, and the energy-loss scale was calibrated to within ±2 meV by using a second-order polynomial to relate the arrival position of the electrons on the detector to loss energy.

Pulse Radiolysis. This work was carried out at the Brookhaven National Laboratory Laser-Electron Accelerator Facility (LEAF).[30−33] The high-energy electron pulse (less than 50 ps duration) was focused into a quartz cell with a 20 mm optical path length containing sample solutions under argon, and produced solvent cations and solvated electrons. In DCE, solvent cations $DCE^{+\bullet}$ reacted with **1** to produce $\mathbf{1}^{+\bullet}$. In THF, solvated electrons reacted with **1** to produce $\mathbf{1}^{-\bullet}$. The monitoring light source was a pulsed xenon arc lamp. Wavelengths were selected using 10 nm bandpass interference filters. Transient absorption signals were detected with either silicon (EG&G FND-100Q, ≤1000 nm) or InGaAs (GPD Optoelectronics GAP-500 L, ≥1100 nm) photodiode and digitized with LeCroy 8620A-oscilloscope giving 2 ns time resolution.

For $\mathbf{1}^{+\bullet}$ the extinction coefficient was obtained using a previously described procedure[33] that relies on the extinction coefficient of tritolylamine radical cation as a reference. Molar extinction coefficients of radical anions are ordinarily estimated using the homogeneous yield $G(e^-_{THF}) = 0.60$ for electrons in THF,[34−36] where G is the radiation chemical yield (molecules produced/100 eV), with dosimetry relative to a standard aqueous solution. This procedure was not applicable to $\mathbf{1}^{-\bullet}$, for which geminate ions did not decay with diffusion-controlled rates. Instead, the measured rate of electron attachment to **1** was included in the scheme described by Asaoka, et al.[37] along with the electron yields reported by De Waele, et al.[38] The absolute extinction coefficients are estimated to be uncertain by ≃20%.

Single Crystal X-Ray Diffraction. Crystals of **1** were grown by cyclohexane/diethyl ether vapor diffusion at room temperature over a period of days. A crystal of appropriate size was mounted on a glass fiber using Paratone-N oil, transferred to a Siemens SMART diffractometer/CCD area detector, centered in the beam (Mo Kα = 0.710 73 Å; graphite monochromator), and cooled to −134(2) °C by a nitrogen-flow low-temperature apparatus. Preliminary orientation matrix and cell constants were determined by collection of 60 10-s frames, followed by spot integration and least-squares refinement. A minimum of a hemisphere of data was collected using 0.3° ω scans. The raw data were integrated and the unit cell parameters refined using SAINT.[39] Data analysis was performed using XPREP.[40] Absorption correction was applied using SADABS.[41] The data were corrected for Lorentz and polarization effects, but no correction for crystal decay was applied. Structure solutions and refinements were performed on F2 using the SHELXTL[42] software package. All non-H atoms were refined anisotropically. Hydrogens were placed in idealized positions and were included in structure factor calculations but were not refined.

Calculations. Parameters and procedures for the semiempirical PPP[43,44] calculations followed prior work.[45] Core integrals β_{rs} of the bonds between the phenyl groups and the heterocyclic ring were multiplied by the cosine of the twist angle (23°). All singly excited configurations were considered. B3LYP/6-311G* calculations of ground state optimized geometry and vibrational frequencies were performed with Gaussian98.[46] The initial

geometries were based on the X-ray structure and the optimizations were then constrained to C_2 or C_s symmetry.

The ground state geometry was also optimized with the RI-B3LYP method[47−52] and at the RI-CC2[53−55] level with TZVPP[56] basis set, with RI-MP2[57] using the TZVP[56] basis set, in the Turbomole[58] program, version 5.9, and further, at the CAS(12,12)/ANO-S-VTZP[59] level, using version 7.2 of the MOLCAS[60] program. The excited and ionized states of **1** in C_2 symmetry, S_1(1B), S_2(2A), T_1(1B), D^+(1A), and D^-(1B), were optimized at the RI-CC2[61,62]/TZVPP level with the Turbomole program. Excitations from the ground and first singlet and triplet excited states of **1**, and from the ground states of its cation and anion radicals, were calculated using the CC2 model. Excitation energies from the S_0, S_1, and T_1 states were calculated from the S_0 ground state closed shell coupled cluster wave function (in CC2 approximation). Since all CC2 excitation energies were too high by approximately 3000 cm^{-1}, for easier comparison with the observed spectra shown in the figures they were reduced by this amount. The actually calculated uncorrected values are listed in tables.

Transition moment calculation[63,64] is implemented only between the ground and excited states. Therefore, the oscillator strengths for S_1 and T_1 excitations were calculated in a separate run with S_1 and T_1 as the initial state, described by unrestricted orbitals occupied so as to give it B symmetry. The oscillator strength was calculated in the length gauge. Excitation state energies and the transition moments for the radical ion states were calculated directly as linear response from the unrestricted radical ground state.

Results

Ground State Geometry from X-Ray Diffraction (Table 1). The ground state structure was already reported briefly.[15] The single crystal analyzed had a monoclinic cell of dimensions $\alpha = 90.00$, $\beta = 106.472(2)$, $\gamma = 90.00$, $a = 12.8954(10)$ Å, $b = 5.5486(4)$ Å, $c = 20.0322(15)$ Å. The symmetry cell setting was *g* and the HM space group was *P*2/*c*. Only the C_2 conformer was present (Figure 2), and its bond lengths, valence angles and dihedral angles ω are listed in Table 1. The dihedral angles are those between planes fitted through the atoms of isobenzofuran and a phenyl ring.

Calculated Geometry of the Ground State (Table 1). Inspection of formula **1** and analogy to biphenyl suggest that there will be two conformers differing in the relative sense of twist of the phenyl substituents out of the aromatic plane, and this is confirmed by ab initio and DFT calculations. The average deviation of phenyl ring atoms from a fitted plane is less than 0.002 Å, both in experimental and in calculated geometries. The isobenzofuran moiety is distorted slightly more and the average deviation is twice larger. The phenyl rings are calculated to be twisted 21−32° out of the isobenzofuran plane. In the C_2 conformer, the two phenyl groups are twisted in a disrotatory fashion, and a 2-fold symmetry axis passes through the oxygen atom. In the C_s conformer, they are twisted in a conrotatory fashion, and the oxygen atom lies in a mirror plane. In all other respects, the calculated geometries of the two conformers are nearly identical. Their calculated energies are essentially the same and we expect both to be represented almost equally in isotropic solutions at all temperatures of interest.

Calculated Geometries of Excited and Ionized States. Table 2 lists the geometrical parameters calculated for the C_2 conformer of **1** excited into its lowest excited singlet state S_1 (symmetry B) and the next higher singlet S_2 (symmetry A), and into its lowest triplet state T_1. The geometries of the radical cation resulting from a removal of an electron ($\mathbf{1}^{+\bullet}$) and the radical anion resulting from the addition of an electron ($\mathbf{1}^{-\bullet}$) are listed as well.

TABLE 1: Ground State Geometry of 1 (Å and deg; See Figure 2), C_2 Conformer (C_s in Parentheses)

parameter	X-ray	RI-CC2/ TZVPP	RI-MP2/ TZVP	RI-B3LYP/ TZVPP	CAS(12/12)/ ANO-S-VTZP
a	1.430 (3)	1.421 (1.421)	1.417	1.427	1.451
b	1.357 (3) 1.353 (3)	1.379 (1.379)	1.379	1.365	1.359
c	1.422 (3) 1.427 (3)	1.415 (1.415)	1.411	1.421	1.441
d	1.445 (3)	1.444 (1.444)	1.438	1.446	1.444
e	1.378 (3) 1.375 (3)	1.398 (1.399)	1.402	1.389	1.369
f	1.375 (3) 1.374 (3)	1.370 (1.370)	1.358	1.360	1.352
g	1.461 (3) 1.459 (3)	1.443 (1.443)	1.443	1.450	1.466
h	1.392 (3) 1.395 (3)	1.406 (1.406)	1.404	1.404	1.384
i	1.385 (3) 1.386 (3)	1.393 (1.393)	1.391	1.387	1.402
j	1.380 (4) 1.375 (4)	1.396 (1.396)	1.394	1.391	1.367
k	1.383 (4) 1.389 (4)	1.397 (1.397)	1.395	1.392	1.403
l	1.394 (3) 1.383 (3)	1.391 (1.391)	1.390	1.386	1.365
m	1.394 (3) 1.389 (3)	1.407 (1.407)	1.405	1.405	1.413
α	121.5 (2) 121.9 (2)	121.5 (121.5)	121.5	121.4	121.7
β	118.8 (2) 118.7 (2)	118.4 (118.4)	118.3	118.9	118.5
γ	119.7 (2) 119.5 (2)	120.1 (120.1)	120.2	119.6	119.8
δ	106.4 (2) 106.9 (2)	106.6 (106.6)	106.5	106.6	106.3
ε	109.0 (2) 108.9 (2)	108.4 (108.4)	108.2	108.0	108.9
ζ	108.7 (2)	110.0 (110.0)	110.6	110.7	109.7
η	135.2 (2) 135.5 (2)	134.8 (134.8)	134.6	135.2	134.3
θ	120.8 (2) 121.0 (2)	120.6 (120.6)	120.6	121.4	121.5
κ	120.6 (2) 120.4 (2)	120.4 (120.4)	120.4	120.8	120.5
λ	120.4 (2) 120.4 (2)	120.4 (120.4)	120.4	120.5	120.2
μ	119.7 (2) 119.8 (2)	119.5 (119.5)	119.5	119.3	119.7
ν	120.2 (2) 119.9 (2)	120.5 (120.5)	120.5	120.5	120.5
ξ	120.2 (2) 121.0 (2)	120.4 (120.4)	120.3	120.8	120.4
π	118.8 (2) 118.5 (2)	118.9 (118.8)	118.9	118.1	118.6
ω	23.8 24.2	23.5 (24.6)	24.4	21.2	32.4

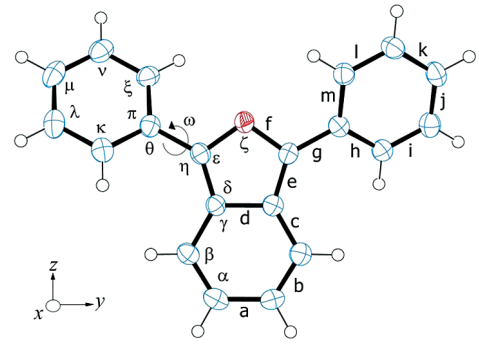

Figure 2. Single-crystal X-ray structure of the C_2 conformer of **1**. Ellipsoids drawn at 50%.

TABLE 2: Optimized RICC2/TZVPP Geometries of Excited and Ionized States of the C_2 Conformer of 1 (See Figure 2)

parameter	S_0 (1A)	S_1 (1B)	S_2 (2A)	T_1 (1B)	D^+ (1A)	D^- (1B)
a	1.421	1.388	1.433	1.380	1.410	1.400
b	1.379	1.414	1.403	1.418	1.388	1.392
c	1.415	1.402	1.391	1.388	1.405	1.412
d	1.444	1.442	1.473	1.432	1.427	1.431
e	1.398	1.421	1.438	1.440	1.418	1.410
f	1.370	1.389	1.378	1.398	1.367	1.385
g	1.443	1.415	1.412	1.410	1.428	1.419
h	1.406	1.418	1.423	1.420	1.400	1.412
i	1.393	1.387	1.391	1.387	1.374	1.376
j	1.396	1.400	1.397	1.400	1.387	1.390
k	1.397	1.400	1.408	1.400	1.388	1.391
l	1.391	1.387	1.385	1.386	1.373	1.374
m	1.407	1.421	1.419	1.422	1.401	1.415
α	121.5	121.4	120.9	120.9	121.4	121.1
β	118.4	118.1	118.8	118.8	117.9	119.0
γ	120.1	120.4	120.2	120.3	120.6	119.9
δ	106.6	106.2	105.9	106.8	106.6	107.0
ε	108.4	110.2	108.7	109.2	108.4	108.5
ζ	110.0	107.2	110.5	108.1	109.9	109.0
η	134.8	134.4	134.6	134.7	134.8	134.8
θ	120.6	121.5	120.5	122.1	120.3	123.0
κ	120.4	120.3	120.0	120.5	119.9	121.2
λ	120.4	120.7	120.8	120.7	119.9	121.8
μ	119.5	119.6	119.6	119.4	120.7	117.6
ν	120.5	120.6	120.4	120.7	119.9	121.7
ξ	120.4	120.4	120.5	120.6	119.8	121.2
π	118.9	118.5	118.7	118.1	119.8	116.6
ω	23.5	9.9	14.0	9.1	22.7	6.7

Electronic Excitation. Because of the out-of-plane twist of the two phenyl groups, the distinction of π and σ symmetry orbitals is only approximate, and so is the reference to the observed transitions as $\pi\pi^*$. In the C_2 conformer, these transitions can be polarized either along the 2-fold axis (z in formula **1**, excited states of A symmetry) or in a plane perpendicular to it (excited states of B symmetry). Transitions into those B states in which transverse electronic excitations within the two phenyl groups do not participate significantly are expected to be polarized nearly exactly along the line that connects the para positions of the two phenyl substituents (y axis in formula **1**). We expect this to include all transitions located at energies lower than ~30 000 cm^{-1}. In the C_s conformer, $\pi\pi^*$ transitions can be polarized perpendicular to the plane of symmetry (y axis in formula **1**, excited states of A" symmetry) or in the plane of symmetry (excited states of A′ symmetry). For low-energy transitions (<~30 000 cm^{-1}), we expect the polarization for transitions into A′ states to lie nearly exactly along the z axis of formula **1**.

All calculations that we have performed, even for higher energy states, yield transition moment directions that deviate from the y or z axes by at most a few degrees. In the following, we therefore describe the results in terms appropriate for a planar molecule of C_{2v} symmetry, with $\pi\pi^*$ transitions polarized along y or z.

Absorption from S_0 and Emission from S_1. Parts A and C of Figure 3 show the room-temperature absorption, fluorescence, fluorescence excitation, and MCD spectra of **1** in CH. Part D shows its low-temperature (77 K) absorption, fluorescence, and fluorescence excitation spectra in 3-MP along with the anisotropy of fluorescence and fluorescence excitation. Parts B and F show the results of calculations. The peak absorption coefficient of **1** in DMSO is 2.5×10^3 M^{-1} cm^{-1}, in close agreement with previous measurements.[22] The fluorescence quantum yield is 0.96 ± 0.03 in all solvents tested. This implies nearly equal quantum yields of ~1 for both conformers present, if they are indeed present in comparable quantities as suggested by the calculations. Therefore, all spectra shown in Figure 3 refer to an average of the spectra of the conformers.

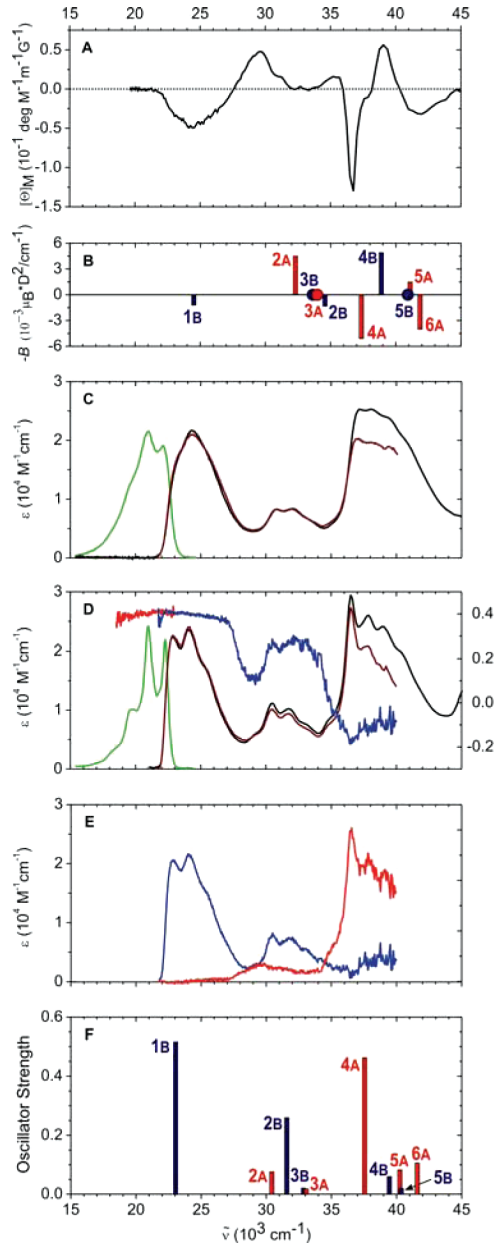

Figure 3. Spectra of **1**. (A) MCD in CH (rt). (B) PPP calculation. Bar height indicates the value of the B term, bar color the polarization (blue, y; red, z). (C) Absorption (black), fluorescence (green), and fluorescence excitation (red) in CH (rt). (D) Absorption (black), fluorescence (green), fluorescence excitation (red), fluorescence anisotropy (bright red), and fluorescence excitation anisotropy (blue) in 3-MP (77 K). (E) Absorption in 3-MP (77 K) decomposed into its y-polarized (blue) and z-polarized (red) components. (F) CC2/TZVPP calculation (all transitions have been shifted to the lower values by 3000 cm^{-1}). Bar length indicates the oscillator strength of y-polarized (blue) and z-polarized (red) transitions.

The shape of the first absorption band, as measured by the ratio of the intensities of the first two vibrational peaks from a Gaussian fitting, is independent of the solvent, while that of the fluorescence depends somewhat on solvent polarity. The fitted peaks are 10−15% narrower in emission than in absorption. The photophysical data for **1** are collected in Table 3.

Analysis of Fluorescence Polarization. Part E of Figure 3 shows the decomposition of the low-temperature absorption

TABLE 3: Photophysical Properties of 1[a]

solvent	$\tilde{\nu}_{abs}$, 10^3cm^{-1} ± 0.03	Γ_{0-1}(abs) ± 0.04	$\tilde{\nu}_F$, 10^3 cm^{-1} ± 0.03	Γ_{0-1}(fl) ± 0.02	Φ_F ± 0.03	k_F, ns^{-1} ± 0.008	$\tilde{\nu}_{T-T}$, 10^3 cm^{-1} ± 0.06	k_T, ms^{-1} ± 0.5
CH	24.33	0.69	22.32	0.66	0.95	0.154	22.12	6.8
THF	24.21	0.67	22.17	0.70	0.99	0.150	22.12	4.9
AN	24.36	0.71	22.12	0.57	0.98	0.132	22.08	3.9
DMSO	24.04	0.59	21.83	0.60	0.97	0.175	21.98	5.4
TOL	24.15	0.69	22.03	0.75	0.99	0.156	22.12	5.0
DMF	24.15	0.66	22.03	0.61	0.96	0.147	22.03	4.2

[a] Peak location in ground state absorption $\tilde{\nu}_{abs}$, in corrected fluorescence $\tilde{\nu}_F$, and in triplet absorption $\tilde{\nu}_{T-T}$; the ratio of intensities of the first to the second peak in absorption Γ_{0-1}(abs) and corrected fluorescence Γ_{0-1}(fl) obtained from fitting of the former with three and the latter with four Gaussians; the fluorescence quantum yield Φ_F and rate constant k_F; and the rate constant of triplet decay k_T.

spectrum into absorption polarized along y and absorption polarized along z. This relies on the above assumption that the absorption intensity polarized along x is negligible, since all observed transitions are effectively of the $\pi\pi^*$ type.

The fluorescence excitation anisotropy surface $R(\tilde{\nu}_1, \tilde{\nu}_2)$ is two-dimensional in that it depends on the excitation wavenumber $\tilde{\nu}_1$ and the fluorescence monitoring wavenumber $\tilde{\nu}_2$. However, we found that in our case $R(\tilde{\nu}_1, \tilde{\nu}_2)$ is nearly independent of the value of $\tilde{\nu}_2$, and is effectively only a function of ν_1. The curve shown in part D of Figure 3 was recorded at $\tilde{\nu}_2 = 20{,}830$ cm^{-1} and the near independence of R of the value of $\tilde{\nu}_2$ is illustrated in the fluorescence anisotropy curve excited in the region of the first transition, at $\tilde{\nu}_1 = 23\,260$ cm^{-1}. This is essentially constant, $R(\tilde{\nu}_1, \tilde{\nu}_2) = 0.38$, for any $\tilde{\nu}_1$ in the region of the first transition and any $\tilde{\nu}_2$, demonstrating that the intense first absorption band and the fluorescence are purely polarized along the same axis. In principle, this could be y or z, but all methods of quantum chemical calculation agree that the correct choice is y, and this is assumed in the following. The dips in the anisotropy curve near 28 000 and 35 000 cm^{-1} suggest that z-polarized transitions occur at these energies. As first shown by Albrecht,[65] in favorable cases it is possible to derive the two purely polarized spectral curves $A_y(\tilde{\nu}_1)$ and $A_z(\tilde{\nu}_1)$ quantitatively from the absorption spectrum $A(\tilde{\nu}_1)$ and the fluorescence anisotropy $R(\tilde{\nu}_1, \tilde{\nu}_2)$.

We use the general formula[26d]

$$R(\tilde{\nu}_1,\tilde{\nu}_2) = (3/5)\left[\sum_u r_u(\tilde{\nu}_1)\, q_u(\tilde{\nu}_2) - 1/3\right] \qquad (1)$$

where the sum runs over $u = x, y, z$, $r_u(\tilde{\nu}_1)$ is the fraction of absorption at $\tilde{\nu}_1$ polarized along u and $q_u(\tilde{\nu}_2)$ is the fraction of emission at $\tilde{\nu}_2$ polarized along u. As noted above, $q_y = 1$, $q_x = q_z = 0$ for all values of $\tilde{\nu}_2$, hence

$$\begin{aligned} A_y(\tilde{\nu}_1) &= [(5/3)R(\tilde{\nu}_1) + 1/3](\tilde{\nu}_1) \\ A_z(\tilde{\nu}_1) &= [2/3 - (5/3)R(\tilde{\nu}_1)]A(\tilde{\nu}_1) \end{aligned} \qquad (2)$$

The resulting purely polarized absorption curves $A_y(\tilde{\nu}_1)$ and $A_z(\tilde{\nu}_1)$ are shown in part E of Figure 3. As noted, they are the weighted averages of the spectra of the two conformers. Specifically, it is clear that the first absorption band is purely polarized in both conformers. We accept the computational result that the transition moment is directed along the molecular y axis, but the following interpretation of LD results would not change if it were polarized along z.

Linear Dichroism. Independent determination of the purely polarized absorption curves was sought from an LD measurement on **1** dissolved in stretched polyethylene. This turned out to be impossible, because the two conformers of **1** orient to different degrees. Instead, the results provided evidence that the two anticipated conformers are indeed present. In the region of the purely polarized first transition, it also provided their separate absorption spectra. It is probably not a coincidence that the spectra of solid films of **1** deposited under various conditions differ from each other noticeably in this same spectral region and give different yields of singlet fission.[19] This could be an indication that microcrystals of the two conformers undergo singlet fission at different rates, and we have decided to examine the conformers in some detail.

The LD spectrometer produces the absorbance $A(\tilde{\nu}) = [E_Z(\tilde{\nu}) + E_Y(\tilde{\nu})]/2$ and the linear dichroism $LD(\tilde{\nu}) = E_Z(\tilde{\nu}) - E_Y(\tilde{\nu})$, where Z is the polymer stretching direction, Y is perpendicular to Z (in a uniaxial sample, all possible choices of Y are equivalent), and X is the light propagation direction. These results provide access to the parallel polarized $E_Z(\tilde{\nu})$ and perpendicular polarized $E_Y(\tilde{\nu})$ absorption curves. For weakly dichroic samples, this process is more accurate than separate measurements of $E_Z(\tilde{\nu})$ and $E_Y(\tilde{\nu})$ with linearly polarized light.

For molecules such as **1**, with negligible absorption polarized along x and all transition moments directed along either along y or along z, the purely polarized absorption curves $A_y(\tilde{\nu})$ and $A_z(\tilde{\nu})$ can be deduced if the solute is partially aligned and if it is possible to discern spectral features associated with the y and z transition moment directions.[26e] We start with

$$\begin{pmatrix} E_Y(\tilde{\nu}) \\ E_Z(\tilde{\nu}) \end{pmatrix} = \begin{pmatrix} (1 - K_y)/2 & (1 - K_z)/2 \\ K_y & K_z \end{pmatrix} \begin{pmatrix} A_y(\tilde{\nu}) \\ A_z(\tilde{\nu}) \end{pmatrix} \qquad (3)$$

where the orientation factors $K_y = \langle\cos^2(Z,y)\rangle$ and $K_z = \langle\cos^2(Z,z)\rangle$ are measures of the average angle (Z, y) and (Z, z) between the laboratory Z axis and the molecular y or z axis, respectively. In the IR region, x-, y-, and z-polarized transitions are typically all available. The validity of the relation $\Sigma_u K_u = 1$ (u runs over x, y, and z) has been verified in numerous cases[66] and is compatible with the uniaxial nature[26f] of stretched polyethylene sheets.

When K_y and K_z are known and different from each other, purely polarized spectra $A_z(\tilde{\nu})$ and $A_y(\tilde{\nu})$ are

$$\begin{pmatrix} A_y(\tilde{\nu}) \\ A_z(\tilde{\nu}) \end{pmatrix} = (K_z - K_y)^{-1} \begin{pmatrix} 2K_z & K_z - 1 \\ -2K_y & 1 - K_y \end{pmatrix} \begin{pmatrix} E_Y(\tilde{\nu}) \\ E_Z(\tilde{\nu}) \end{pmatrix} \qquad (4)$$

In practice, $A_y(\tilde{\nu})$, $A_z(\tilde{\nu})$, K_y, and K_z are obtained simultaneously by a trial and error procedure in which families of linear combinations of the observed spectra $E_Z(\tilde{\nu}) - cE_Y(\tilde{\nu})$ are plotted and inspected until the values of c are found for which one of the other set of spectral features disappears, e.g., c_y for y-polarized and c_z for z-polarized features. These particular linear combinations are then proportional to the purely polarized spectra $A_z(\tilde{\nu})$ and $A_y(\tilde{\nu})$, respectively, and $K_u = c_u/(2 + c_u)$, $u = y, z$.

From eq 2, $E_Y(\tilde{\nu})$ and $E_Z(\tilde{\nu})$ should be proportional to each other if $K_y = K_z$, and also in all spectral regions in which absorption is either purely y-polarized or purely z-polarized. This

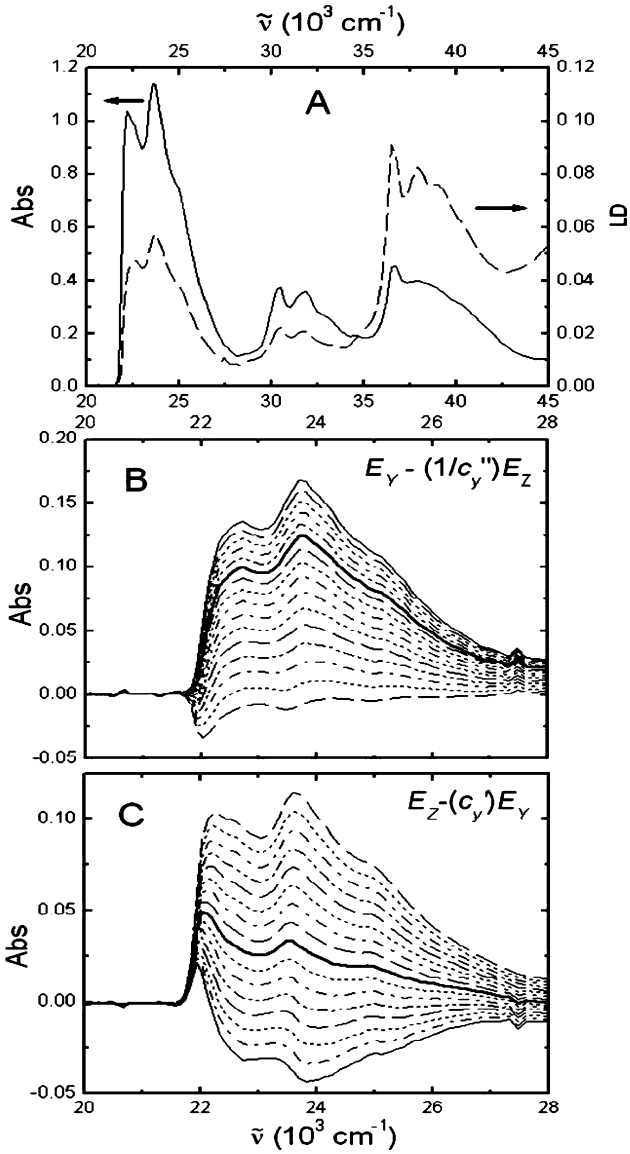

Figure 4. (A) Absorption (left scale) and linear dichroism (right scale) of **1** in stretched polyethylene at liquid N_2 temperature. (B, C) Families of linear combinations of E_Z and E_Y in which the coefficient c varies in steps of 0.04. The value of c_y'' ranges from 1.20 to1.80, and the value of c_y' ranges from 1.00 to 1.30.

expectation is generally found to be well fulfilled. The minute deviations that have been observed for some compounds have been attributed to slight differences in the degree of orientation of solute molecules located in different sites and therefore possessing slightly different excitation energies or to the birefringence of the orienting medium.[26g] Since the excitation energy of a transition observed in a dielectric medium is reduced as the index of refraction is increased, and the index is slightly higher for light polarized along the laboratory Z axis than the Y axis, the measured $E_Z(\tilde{\nu})$ spectrum appears slightly displaced to lower energy from the $E_Y(\tilde{\nu})$ spectrum. This may cause an appearance of a small derivative-shaped "wiggle" at the onset of absorption bands in $A_z(\tilde{\nu})$ and $A_y(\tilde{\nu})$ spectra that are deduced from the LD experiment.

Although the first transition band of both presumably present conformers of **1** is purely polarized, the first observed band has a slightly but unmistakably and reproducibly different shape in $A(\tilde{\nu})$ and in LD($\tilde{\nu}$) (Figure 4, part A), and therefore also in E_Z and E_Y (Supporting Information, Figure S1). Parts B and C of Figure 4 demonstrate that it is impossible to find a linear combination of E_Z and E_Y in which all of the first band is absent. The discrepancy is much larger than those normally attributed to the effects of birefringence mentioned above. Most importantly, it has the wrong sign, with the $E_Y(\tilde{\nu})$ spectrum displaced to slightly lower energies from the $E_Z(\tilde{\nu})$ spectrum (Figure S1). In the higher energy region, near 30 000 cm^{-1}, it also is impossible to find linear combinations that would reproduce the purely polarized $A_z(\tilde{\nu})$ and $A_y(\tilde{\nu})$ spectra of Figure 3.

This result demonstrates the presence of two species with slightly different spectra. In principle, it is possible that both actually are the same conformer and differ in the nature of the site into which they are absorbed within the stretched polymer. However, we consider it unlikely that intermolecular interactions could cause as much difference in the spectral shapes of the first transition in the two species as is observed in Figure 4 and propose that these LD results actually provide experimental evidence for the presence of two conformers of **1**. By far the largest difference between the conformers is their molecular shape, and this is the property known to dictate the degree of orientation of aromatics in stretched polyethylene.[26h,66−68]

In regions of mixed polarization, one cannot deduce four purely polarized overlapping spectra from the two observed linearly independent spectra available on a uniaxial sample. However, in the region of the first band, where $A_z'(\tilde{\nu}) = A_z''(\tilde{\nu}) = 0$, eq 3 becomes

$$\begin{pmatrix} E_Y(\tilde{\nu}) \\ E_Z(\tilde{\nu}) \end{pmatrix} = \begin{pmatrix} (1 - K_y')/2 & (1 - K_y')/2 \\ K_y' & K_y'' \end{pmatrix} \begin{pmatrix} A_y'(\tilde{\nu}) \\ kA_y''(\tilde{\nu}) \end{pmatrix} \quad (5)$$

where the unknown factor k corrects for a possibly significant difference in the concentrations of the two species present in the stretched polyethylene environment. We label them with a prime and a double prime.

Unless the orientation factors K_y' and K_y'' are equal, matrix inversion yields an expression for the absorption spectra of the two species,

$$\begin{pmatrix} A_y'(\tilde{\nu}) \\ kA_y''(\tilde{\nu}) \end{pmatrix} = (K_y'' - K_y')^{-1} \begin{pmatrix} 2K_y'' & K_y'' - 1 \\ 2K_y' & 1 - K_y' \end{pmatrix} \begin{pmatrix} E_Y(\tilde{\nu}) \\ E_Z(\tilde{\nu}) \end{pmatrix} \quad (6)$$

Using the stepwise reduction procedure, we find that the sharp first peak at low energy disappears in the combination $-(1/c_y'')E_Z(\tilde{\nu}) + E_Y(\tilde{\nu})$ when $c_y'' = 1.56 \pm 0.02$. This spectral curve is proportional to $A_y'(\tilde{\nu})$. The shoulder on the high-energy side of this peak disappears in $E_Z(\tilde{\nu}) - c_y'E_Y(\tilde{\nu})$ when $c_y' = 1.16 \pm 0.04$, and this curve is proportional to $A_y''(\tilde{\nu})$. The orientation factors that describe the average orientation of the molecular y axis are $K_y' = c'/(2 + c') = 0.37 \pm 0.01$ for the primed conformer and $K_y' = c''/(2 + c'') = 0.44 \pm 0.005$ for the double primed conformer. The latter thus orients significantly better than the former. In the absence of a reliable calculation of the shape of the Franck−Condon envelope of the first transition in the two conformers, we are unable to tell which spectrum belongs to the C_2 and which to the C_s conformer. The spectra of the two conformers shown in bold lines in Figure 4 are not on the same scale, and a normalization is impossible since we do not know their relative concentrations in the stretched polymer.

Excitation from the S_1 State. Information about higher excited singlet states can be accessed by transient absorption spectroscopy of the first excited singlet state S_1. The spectrum obtained by femtosecond pump−probe spectroscopy in DMSO is shown in Figure 5. It decays in a single exponential fashion,

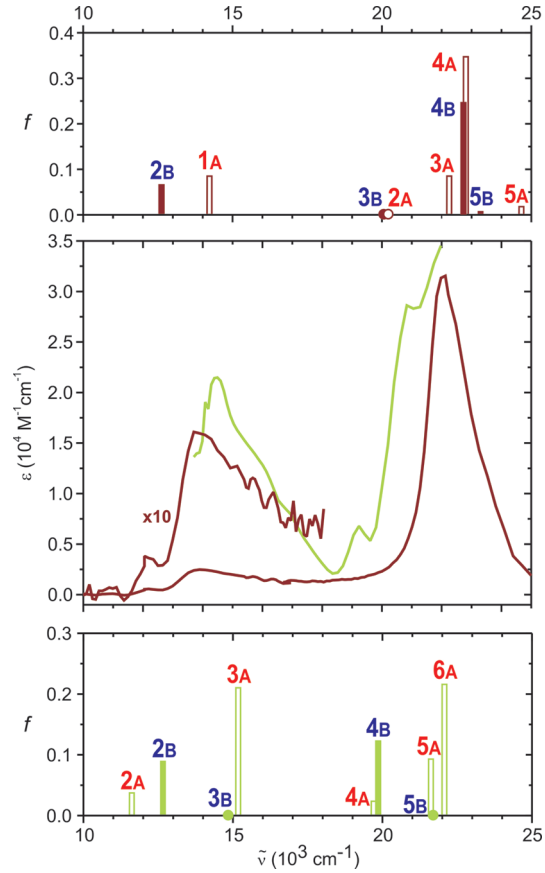

Figure 5. Transient absorption spectra of the first excited singlet (S_1, chartreuse, $\tau = \sim 5$ ns) and the first triplet (T_1, brown, $\tau = \sim 230$ μs) of **1** in DMSO.

with a lifetime of 5.0 ± 0.5 ns, which agrees within experimental uncertainty with the fluorescence lifetime measured by single photon timing, 5.6 ± 0.3 ns. The absorption coefficient of the strong peak at ~14 500 cm^{-1} was determined from ground state depletion to be ~23 400 M^{-1} cm^{-1} with very limited accuracy, due to unfavorable peak overlap.

Singlet State Assignments. The nature of the excited states and of the molecular orbitals involved in the excitations is shown in Figure 6. The MCD spectra of Figure 3A, the purely polarized spectra of Figure 3E and the S_1-S_x spectrum of Figure 5 can now be used to deduce the presence and symmetry of the singlet excited states of **1** (Table 3), and to compare them with the results of CC2 calculations. Most of the transitions yield fairly broad bands, suggesting a considerable change in the equilibrium geometry upon excitation, in keeping with the data shown in Table 2. We consider excited states of B symmetry first. The absorption into the 1B state centered at ~24 000 cm^{-1} and associated with a negative MCD peak (positive *B* term) is the most prominent. The next B symmetry transition is weaker and is centered at ~30 000 cm^{-1}. It has a negative *B* term and is assigned to the 2B state. An even weaker transition with another negative *B* term, centered at ~39 000 cm^{-1} follows, and is assigned to the 4B state, since the CC2 calculation predicts a very weak transition into a 3B state ~1000 cm^{-1} above 2B, not detectable in any of our spectra. In the PPP results, the order of the nearly degenerate 2B and 3B states is inverted. In the observed spectra, the transition into 3B, if present, is presumably buried under the transition assigned to 2B.

The first A symmetry transition is into the 2A state and is located near 29 000 cm^{-1}. Its existence is not apparent in the ordinary absorption spectrum but is obvious from its negative

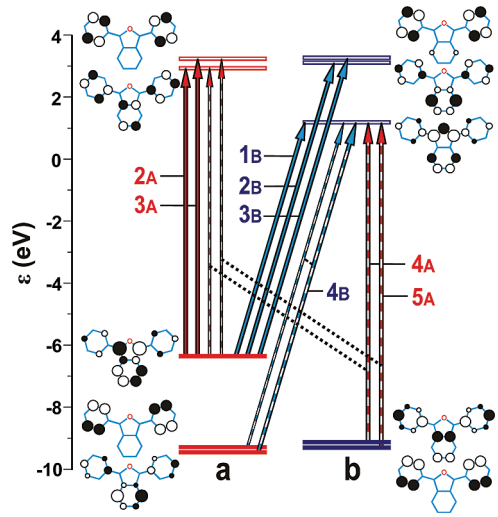

Figure 6. Orbital energies in **1**. Chief contributions to $S_0 \rightarrow S_x$ excitations calculated at the CC2/TZVPP level are shown. Striped arrows indicate that more than one electron promotion has a significant amplitude.

B term in the MCD spectrum and from polarized fluorescence. The transition into the 3A state appears at ~35 000 cm^{-1}. It is clearly present in the MCD spectrum as a positive peak but is relatively indistinct in the polarized absorption spectrum, where it takes the form of a weak shoulder at the foot of the much stronger transition to the 4A state, located at ~37 000 cm^{-1}. The positive *B* term of the *z*-polarized transition into 4A is the dominant feature of the MCD curve. In the absorption spectrum, this transition rivals 1B in prominence. It covers up not only the absorption into the 4B state, which is readily detected due to its opposite *y* polarization and its oppositely signed *B* term, but also the equally *z*-polarized transitions into the next A states. One of these, presumably 6A, according to the PPP calculation, is apparent in the MCD spectrum at ~42 000 cm^{-1}, owing to its strong positive *B* term.

Transitions observed in the S_1-S_x spectrum (Figure 5) originate in the 1B state, and only the strongest ones are likely to be observable. The band at ~15 000 cm^{-1} is assigned to a transition to the 3A state, and the absorption onset near ~22 000 cm^{-1} may be due to a transition to the 6A state, but it is hard to be sure, because of strong interference by stimulated emission.

The CC2 calculated energies (Table 4) are all about ~3000 cm^{-1} too high and in Figures 3, 5, 8, and 10 they have been reduced by this amount to facilitate comparison. The PPP calculated energies are approximately correct and do not require such a shift, except for the transition to the 2A state, which is calculated about 3000 cm^{-1} too high.

Molecular Orbitals and the Perimeter Model. The π MOs of **1** are essentially the same whether calculated for singlet or triplet states or for the radical ions, and whether calculated by an ab initio method or the semiempirical PPP method with single excited configurations. Their form and relative energies can be deduced from the perimeter model[69,70] without any computation,[71] or from the Hückel model. The parent aromatic perimeter is the 10-electron 9-membered ring (cyclononatetraenide), whose MOs are dictated by the 9-fold axis of symmetry. Its frontier orbitals are a doubly degenerate highest occupied MO (HOMO) with two bond-cutting nodal planes and a doubly degenerate lowest unoccupied MO (LUMO) with three such nodal planes. A cross-linking perturbation converts the parent perimeter into the indenide anion, consisting of a fused five- and six-membered ring. Using the 2-fold axis remaining after this symmetry

TABLE 4: Observed and CC2 Calculated Singlet Excitations in 1[a]

	obsd[b]				calcd[c]			
S_x	$\tilde{\nu}$ 10^3cm^{-1}	f[d]	pol[e]	B[f]	$\tilde{\nu}$ 10^3cm^{-1}	f[g]	pol[h]	B[i]
				S_0 (1A) → S_x and S_0 (1A′) → S_x				
1B (1A″)	24.3	0.04	y	2.1	26.0[j] (26.0)	0.52 (0.53)	y (y)	1.2
2A (2A′)	29.6	0.006	z	−0.96	33.4[k] (33.5)	0.076 (0.072)	z (0.58)	−4.5
2B (2A″)	31.1	0.02	y	−0.15	34.6 (34.2)	0.26 (0.26)	y (y)	1.3
3B (3A″)					35.9 (35.7)	0.021 (0.017)	1.95 (y)	0
3A (3A′)	35.4	0.003	z	−0.19	36.0 (36.0)	0.018 (0.019)	z (1.09)	0.1
4A (4A′)	36.7	0.003	z	0.86	40.6 (40.8)	0.46 (0.47)	z (0.63)	5.1
4B (4A″)	39	0.006	y	−0.52	42.4 (42.4)	0.060 (0.058)	1.24 (y)	−4.9
5A (5A′)					43.2 (43.3)	0.082 (0.11)	z (4.69)	−1.5
5B					43.3	0.020	53.1	−0.5
6A	42			0.6	44.6	0.11	z	4.0
6B					49.4	0.018	y	−0.3
7A					49.5	0.015	z	
	obsd.[b]				S_1 (1B) → S_x	calcd.[m]		
1A (S_0)					−15.1	0.36	y	
2B					13.9	0.090	z	
2A					14.1	0.037	y	
3A	∼14.5	∼0.2			16.5	0.21	y	
3B					19.3	0.0041	z	
4A					19.8	0.024	0.15	
4B					20.6	0.12	z	
5A					22.0	0.094	0.01	
6A	∼22				25.6	0.22	y	
5B					27.1	0.0060	z	
6B					29.8	0.00026	z	
7B					31.4	0.096	z	

[a] State symmetry assignments are based on calculations, and for low-energy S_0 → S_1 transitions they agree with experimental relative symmetries. [b] Absorption peak positions in 3-MP at 77 K. [c] Calculated vertical excitation energies of the C_2 conformer (in parentheses, the C_s conformer) at the equilibrium geometry of the initial state. [d] Oscillator strength in 3-MP at 77 K. Because of transition overlap, the values are only approximate. [e] Polarization direction from polarized fluorescence, assuming that all absorption and emission is y or z polarized ($\pi-\pi^*$) and that the first transition is polarized along y. [f] MCD B term in cyclohexane at room temperature in units of 10^{-3} (Debye^2 β_e)/cm^{-1}. Because of overlap and mutual cancellation, the real values are undoubtedly larger. [g] Oscillator strength for the C_2 conformer (in parentheses, the C_s conformer). [h] Axis of polarization (see formula **1** or Figure 2) or inclination of the transition moment from y in toward x in deg, for the C_2 conformer. In parentheses, results for the C_s conformer for which the inclination is measured from z toward x. Inclinations smaller than 0.1° were set equal to zero. [i] PPP calculation, in units of 10^{-3} (Debye^2 β_e)/cm^{-1}. States were correlated with CC2 states by inspection of excitation energies, symmetries, intensities, and wave function composition. Results for highest energy states are not shown since such correlation was equivocal. [j] The calculated adiabatic S_0 → S_1 excitation energy is 24.0 × 10^3cm^{-1}. [k] The calculated adiabatic S_0 → S_2 excitation energy is 31.8 × 10^3cm^{-1}. [l] Absorption peak positions in DMSO solvent at room temperature. [m] Calculated vertical excitation energies of the C_2 conformer at the equilibrium geometry of the S_1 state.

reduction, the frontier MOs of the indenide anion can be classified as a and b. Inspection of the perimeter MOs shows that within the HOMO pair, the cross-link strongly stabilizes the b MO and destabilizes the a MO, whereas within the LUMO pair, it destabilizes the a MO and hardly affects the b MO at all. Subsequent replacement of one of the carbons with an oxygen to produce isobenzofuran stabilizes both MOs of a symmetry.

The result of the combined perturbations is an MO sequence 2 (b), 1 (a, HOMO), −1 (b, LUMO), −2 (a), with a large separation between the two bonding orbitals 2 (b) and 1 (a) and a smaller separation between the two antibonding ones, −1 (b) and −2 (a). Such an orbital energy arrangement leads to configuration excitation energies increasing in the order 1, −1; 1, −2; 2, −1; 2, −2, characteristic of a "positive hard MCD chromophore".[71] For excitations from the ground state of such a chromophore, one expects (i) first a low-energy L_1 transition dominated by the 1, −1 electron promotion, with a positive MCD B term, (ii) second, an L_2 transition with strong 1, −2 and some 2, −1 character and a negative B term, (iii) third, a B_1 transition with strong 2, −1 and some 1, −2 character and a positive B term, and (iv) finally, a rarely observed high-energy B_2 transition with a negative B term.[72]

The introduction of the two phenyl substituents into isobenzofuran to produce **1** produces the MOs obtained in our calculations. We number them sequentially, separately for a and b symmetry orbitals. We use positive numbers for MOs occupied in the S_0 state of **1**, starting with the HOMO (a1), and negative numbers for MOs vacant in the S_0 state of **1**, starting with the LUMO (−1b). Their calculated form and energy order are the same in all cases except that in the radical anion $\mathbf{1}^{-\bullet}$ the order of the nearly degenerate −2b and −3b MOs is interchanged.

The perturbation by the two phenyl substituents leaves the 1 (a) HOMO and the −1 (b) LUMO of isobenzofuran essentially intact, and the MOs 1a and −1b of **1** are concentrated on the parent perimeter (Figure 6). In contrast, the substitution has a dramatic effect on the lower energy MO 2 (b) and the higher energy MO −2 (a) of the isobenzofuran system, because the frontier orbitals of the phenyl substituents are of comparable energies and strong mixing takes place. The four HOMOs of the benzene rings mix with MO 2 (b) of isobenzofuran to give a total of five bonding MOs. Four of the resulting MOs are nearly degenerate: 1b, 2b, 2a, and 3a. The MOs 3a and 1b are largely concentrated on the isobenzofuran perimeter with some delocalization onto the phenyls, whereas the MOs 2a and 2b are isolated on the phenyl rings since they carry a node at the carbon atom through which they are attached. The more stable fifth MO (3b) contains mostly perimeter character. Similarly, the four LUMOs of the phenyl substituents mix with the MO −2 (a) of isobenzofuran to give five antibonding MOs.

Four of these MOs, −1a, −2a, −2b, and −3b, are nearly degenerate. The MOs −1a and −2b are largely concentrated on the isobenzofuran perimeter with some delocalization onto the phenyls, whereas the MOs −2a and −3b are isolated on the phenyl rings since they carry a node at the attachment atom. The only exception is $\mathbf{1}^{-\bullet}$, where the β spinorbital −2b is confined to the phenyls and −3b is largely on the perimeter (the α spinorbitals are ordered in the usual fashion). The fifth MO that results from the mixing, −3a, is less stable and does not enter into the description of the low-energy states considered presently.

This increase in the number of MOs in the frontier region complicates the possible low-energy electron promotions, and makes it somewhat harder to relate the states of **1** to those of the parent perimeter. Since the frontier 1a and −1b MOs hardly changed at all upon substitution, the HOMO−LUMO excitation in **1** remains of low energy and clearly represents the L_1 transition in the perimeter model nomenclature. The L_2 character of a transition that was primarily of 1 (a), −2 (a) nature in isobenzofuran will be diluted among three transitions of A symmetry in **1**. Similarly, the B_1 character of the transition that was primarily of 2 (b), −1 (b) nature in isobenzofuran will be diluted among three transitions of A symmetry in **1**.

In spite of this complication, the perimeter state labels can be assigned, and predictions of MCD signs can be made fairly easily, primarily because the frontier orbitals 1a and −1b remained unchanged. Since −1a, one of the three a-symmetry MOs that result from the mixing of substituent orbitals with the MO −2 (a) of isobenzofuran, has much more perimeter character than the MO −2a, the transition from 1a to −1a will be recognizable as producing the L_2 state of **1**. Magnetic mixing of all three states with the L_1 state should produce the same positive sign for the *B* term of L_1 as in isobenzofuran itself, and a negative sign for that of the L_2 state. By the same token, since among the three b-symmetry MOs that resulted from the mixing of substituent orbitals with the MO 2 (b) of isobenzofuran, 1b and 3b have considerably more perimeter character than 2b, the excitations from 1b and 3b to −1b should share the B_1 character in **1**. In the first approximation, magnetic mixing of these states with the B_2 state should contribute positively to the sign of their *B* term, as in benzoisofuran itself.

Description of S_0−S_x Excitations. The excitation amplitudes of the first eleven excited singlet states of **1** calculated by the ab initio CC2 method (Figure 6) and by the simple PPP model with single excitations agree astonishingly well with each other, and the two calculations provide the same interpretation of the nature of the electronic excitations. Both agree with the experimental results and with the simple perimeter model analysis. The PPP results provide a very satisfactory agreement with the MCD signs observed for all of the intense peaks 1B, 2A, 4A, 4B, and 6A. Qualitatively, the electronic transition energies fall into three groups.

The lowest energy group consists of only one transition, from the 1A ground state to the 1B state, described as 1a to −1b (HOMO−LUMO) electron promotion This is the L_1 transition, and it has the expected and calculated positive *B* term in MCD. However, because of the orbital mixing induced by the phenyl substituents, some of the L_1 character is shared with the 2B state.

The next group of transitions from 1A into the 2A, 3A, 2B, and 3B states is related to the L_2 transition in isobenzofuran and can be described as due to electron promotions from 1a into the four nearly degenerate MOs that lie above the LUMO. Excitations into the orbitals −1a and −2a account for the excited states 2A and 3A, respectively, and excitations into −2b and −3b account for the excited states 2B and 3B, respectively. The 2A state captures most of the L_2 character and has the anticipated and also calculated negative *B* term in MCD.

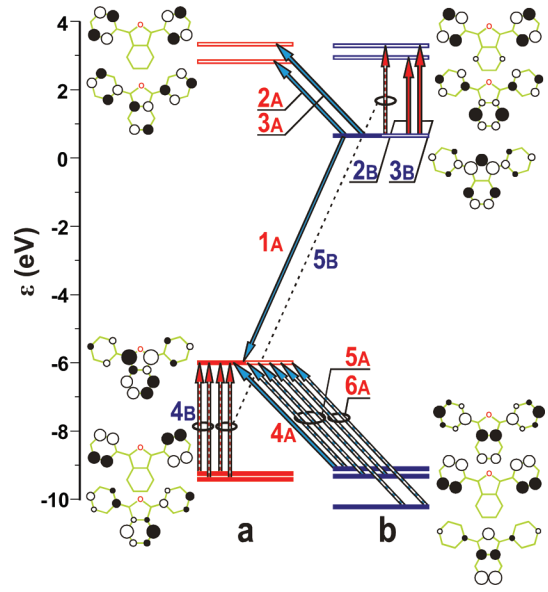

Figure 7. Orbital energies in **1**. Chief contributions to $S_1 \rightarrow S_x$ excitations calculated at the CC2/TZVPP level are shown. Dashed arrows indicate that more than one electron promotion has a significant amplitude.

The high-energy group of electronic transitions comprises excitations from 1A to the 4A, 5A, 6A, 4B, and 5B states and is related to the B_2 transition in isobenzofuran. It is due to electron promotions into the −1b LUMO from the four nearly degenerate MOs that lie below the HOMO and a more stable fifth orbital 3b. Excitations from b symmetry orbitals account for the excited states 4A, 5A, and 6A, and excitations from the a symmetry orbitals account for the excited states 4B and 5B. As expected from the perimeter model, the configurations that dominate the 2A and 4A states mix significantly. Of all these states, the 4A state corresponds most closely to B_1 of the perimeter model, and it has the expected and calculated positive *B* term.

The B_2 state is too high in energy to have appeared in the results of the calculation, and is not observed in the accessible energy range. Its dominant configuration would correspond to an electron promotion from the 1b orbital into the −1a orbital.

Description of S_1−S_x Excitations. A simple one-electron description of excitations from the first excited singlet state 1B (S_1) is shown in Figure 7. In this state, the 1a HOMO and the −1b LUMO of the S_0 state of **1** are both approximately singly occupied and can be referred to as the lower and the upper SOMO. Moving an electron from the latter to the former releases energy in the form of fluorescent emission from the 1B state to the 1A (S_0) ground state. Low-energy absorptions from S_1 correspond to promoting the electron present in the upper SOMO −1b to one of the four nearly degenerate vacant orbitals, −1a, −2a, −2b, and −3b, located just above. MOs of a symmetry yield transitions into 2A and 3A states, and MOs of b symmetry yield transitions into 2B and 3B states. Two of the four transitions are predicted to lie below the region of experimentally accessible energies (1B−2A and 1B−2B). One of the other two (1B−3A) is attributed to the absorption observed near 14 500 cm^{-1}, while the other (1B−3B) is predicted to be inobservably weak.

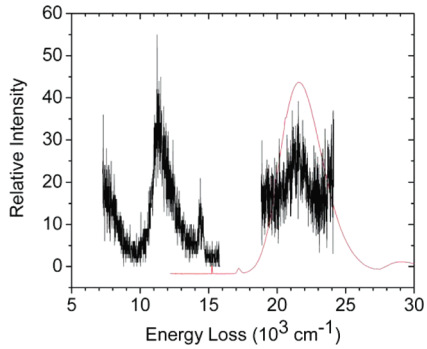

Figure 8. Spectra of **1**. EELS at 2.5 V incident energy (black, neat solid, ~10 K; the small peak near 14 000 cm^{-1} is an irreproducible artifact) and UV absorption (red, CH, rt).

This group of four low-energy transitions is followed by an analogous group of higher energy transitions, which involve promotions of an electron from one of the doubly occupied MOs into the lower SOMO 1a. In four of these transitions, the electron is promoted from one of the four nearly degenerate MOs located just below the lower SOMO, 1b, 2b, 2a, and 3a. The MOs of a symmetry are responsible for the excited states 4B and 5B, and those of b symmetry yield the states 4A and 5A. A fifth excitation into the lower SOMO (1B−6A) is believed to be responsible for the absorption intensity observed near 22 000 cm^{-1}. As shown in Figure 7, the promotion occurs from the next lower MO of b symmetry, the fifth that results from the interactions of the four phenyl substituent orbitals with the 2 (b) MO of the parent perimeter.

As seen in Figure 7, the excitations in this higher energy region are somewhat complicated by configuration mixing. In spite of this, the one-electron description of transitions from both the S_0 and the S_1 states is astonishingly simple.

Triplet State Assignments. We have observed no phosphorescence in a low-temperature glass and have detected no transient triplet−triplet absorption in a laser flash photolysis experiment without a sensitizer. The energy of the lowest triplet has been reported as 11 900 ± 100 cm^{-1} (adiabatic) in benzene solution on the basis of triplet sensitization studies[22] and as 12 900 ± 400 cm^{-1} in DMF on the basis of electrogenerated chemiluminescence.[24] Our electron energy loss spectrum measured on a film of the solid (Figure 8) is noisy but reproducible and yields a relatively sharp peak at 11 400 cm^{-1}. It also shows a weaker band at an energy coincident with that of the first singlet absorption band in the UV spectrum.

The solution T_1-T_x absorption spectrum obtained from laser flash photolysis with anthracene sensitization in DMSO is displayed in Figure 5. The similarity to the S_1-S_x spectrum, which is also shown, is striking. The triplet spectrum contains a weak very broad absorption in the near IR with a maximum at ~13 500 cm^{-1} and strong peak at 21 800 cm^{-1}, with an absorption coefficient of 32 100 ± 3000 M^{-1} cm^{-1}. The triplet decay is first order in the limit of a low concentration of acceptor triplets and the lifetime is ~230 μs.

Vertical triplet excitation energies were calculated by the CC2 method both at the ground state S_0 and at the lowest triplet state T_1 equilibrium geometries. They are listed in Table 5, along with adiabatic triplet excitation energies. The results suggests that the lowest triplet state is 1B and that the low-energy T_1-T_x absorption is due to a superposition of a weaker *z* polarized transition to the 2B triplet state near 12 000 cm^{-1} and a stronger *y*-polarized transition to the 1A state near 14 000 cm^{-1}, both of which can be vaguely discerned in the observed spectrum. The calculated intensities of the following transitions into the 2A and 3B triplet states are too weak for observation. The intense peak at 22 000 cm^{-1} is attributed to an overlap of three intense transitions from 1B to the 3A, 4B, and 4A states and should therefore be of mixed polarization.

Description of T_1-T_x Excitations. A one-electron description of excitations from the first triplet state 1B (T_1) is shown in Figure 9. As in the S_1 state, the HOMO and the LUMO of the S_0 ground state are now both singly occupied and can be referred to as the lower and the upper SOMO. Moving an electron from the latter to the former is no longer possible without change of multiplicity. In all other respects, the description of the transitions is the same as in the singlet manifold, but the degree to which configurations mix is even lower. Low-energy absorptions from T_1 again correspond to promotions of the electron present in the upper SOMO to one of the four nearly degenerate vacant orbitals just above, −1a, −2a, −2b, and −3b. MOs of a symmetry yield the 1A and −2A states, and MOs of b symmetry yield the 2B and 3B states. Higher energy transitions from T_1 again involve promotions of

TABLE 5: Observed and CC2 Calculated Transitions into Triplet States of 1[a]

$S_0 \rightarrow T_x$			T_1 (1B) $\rightarrow T_x$					
	obsd[b]	calcd		obsd[c]		calcd		
T_x	$\tilde{\nu}$ 10^3 cm^{-1}	$\tilde{\nu}$ 10^3 cm^{-1}	T_x	$\tilde{\nu}$ 10^3 cm^{-1}	f[d]	$\tilde{\nu}$ 10^3 cm^{-1}	f[d]	pol[e]
1B (1A″)	11.9	16.5[f] (16.4)	2B	~12		17.6	0.066	*z*
2B (2A″)		28.5 (28.3)	1A	~14[g]	0.025	19.2	0.085	*y*
1A (1A′)		29.5 (29.7)	3B			25.2	0.0054	*z*
2A (2A′)		34.6 (34.6)	1A			25.2	0.0028	0.16
3B (3A″)		34.8 (34.7)	3A			27.3	0.084	*y*
3A (3A′)		35.7 (35.7)	4B	21.8[h]	0.17	27.8	0.24	*z*
4B (4A″)		36.8 (36.8)	4A			27.8	0.35	*y*
4A (4A′)		37.9 (37.9)	5B			30.4	0.0066	*z*
5B (5A″)		38.7 (38.6)	5A			30.6	0.017	1.01
5A (5A′)		39.8 (39.9)						
6B (6A″)		40.6 (40.5)						
6A (6A′)		40.7 (40.7)						

[a] Vertical excitation energies of the C_2 conformer of **1** calculated at the equilibrium geometry of the initial state. For $S_0 \rightarrow T_1$ transitions, symmetries and excitation energies for the C_s conformer are shown in parentheses. State symmetry assignments are based only on calculations. [b] In benzene solvent. [c] In DMSO solvent. [d] Oscillator strength. [e] Axis of polarization (see formula **1** or Figure 2), or inclination of the transition moment from *y* in toward *x* in deg. Inclinations smaller than 0.1° were set equal to zero. [f] The calculated adiabatic $S_0 \rightarrow T_1$ excitation energy is 13.9 × 10^3cm^{-1}. [g] Assigned to overlapping 1B → 2B and 1B → 1A transitions. [h] Assigned to overlapping 1B → 4B and 1B → 4A transitions.

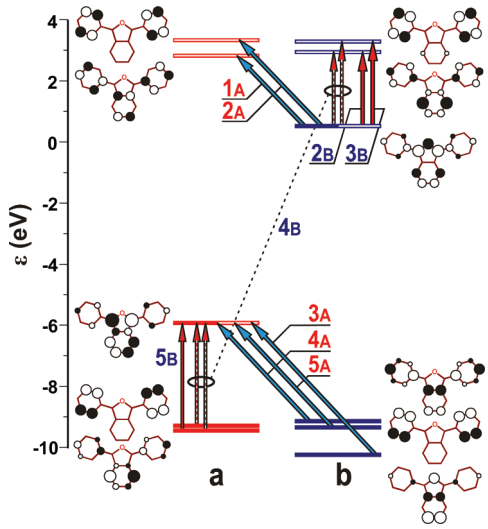

Figure 9. Orbital energies in **1**. Chief contributions to $T_1 \rightarrow T_x$ excitations calculated at the CC2/TZVPP level are shown. Dashed arrows indicate that more than one electron promotion has a significant amplitude.

an electron into the lower SOMO. In four of them, the electron is promoted from one of the four nearly degenerate MOs located just below the lower SOMO, 1b, 2b, 2a, and 3a. The MOs of *a* symmetry yield the 4B and 5B states and those of b symmetry yield the 4A and 5A states. As in the singlet manifold, another excitation in this energy region (1B−3A) is due to an electron promotion from the next lower MO of b symmetry into the lower SOMO. The nearly complete parallelism between the description of the excitations from S_1 and from T_1 accounts for the similarity of the two spectra in Figure 5.

Ionized States. The absorption spectra of the radical cation $\mathbf{1}^{+\bullet}$ and radical anion $\mathbf{1}^{-\bullet}$, produced by pulse radiolysis in DCE and THF solution, respectively, are shown in Figure 10. The observed and calculated electronic excitation energies and intensities are collected in Table 6. The interpretation of the spectra of the radical ions in terms of the molecular orbitals involved is summarized in Figures 11 and 12.

Radical Cation. The absorption spectrum of $\mathbf{1}^{+\bullet}$ (Figure 10) starts with a weak peak near 14 000 cm^{-1} followed by a more intense shoulder at ∼16 000 cm^{-1} and an intense peak at ∼18 500 cm^{-1}, with an absorption coefficient of ∼17 800 ± 3600 M^{-1} cm^{-1}. Comparison with results of CC2 calculations, again reduced by 3000 cm^{-1}, suggests that the first weak peak is due to a transition to a 1B state, the shoulder is due to intensity borrowing by vibronic interaction with the strongest transition, or possibly to one or more of the weak transitions 2A, 3A, and 3B, and the intense peak is due to a transition to the 2B state.

The weak first transition into the 1B state is attributed to electron promotion from the SOMO 1a to the LUMO −1b of the radical cation (Figure 11). This transition is entirely analogous to the HOMO−LUMO (L_1) transition in neutral **1**, which, however, occurs at energies ∼8000 cm^{-1} higher. The interpretation of the excitation into the 2B state is promotion of an electron into the SOMO from 1b. It is thus nearly the same as the excitation into the 4A state in the T_1-T_x spectrum, which is co-responsible for its strongest peak, located 4000 cm^{-1} higher, and the excitation into the 4A state in the S_1-S_x spectrum, calculated ∼2000 cm^{-1} higher. The unobserved transitions in the calculated absorption spectrum of $\mathbf{1}^{+\bullet}$ can be similarly related to transitions in the T_1-T_x spectrum of **1** (Table 7).

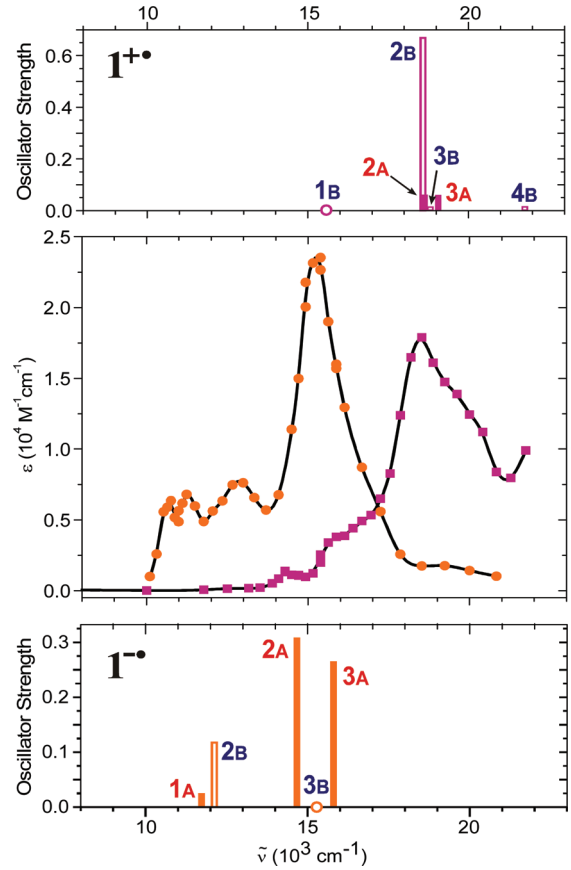

Figure 10. Absorption of the radical anion $\mathbf{1}^{-\bullet}$ (●) and radical cation $\mathbf{1}^{+\bullet}$ (■) obtained by pulse radiolysis of 5 mM **1** in THF and DCE, respectively. CC2/TZVPP calculated spectra on top (cation) and bottom (anion). Full bars: *z* polarization, empty bars: *y* polarization. Calculated transitions have been shifted to the lower energies by 3000 (cation) or 2000 (anion) cm^{-1}.

Radical Anion. Peaks in the absorption spectrum of $\mathbf{1}^{-\bullet}$ occur at much lower energies than was the case for $\mathbf{1}^{+\bullet}$ (Figure 10). A series of three peaks is located at 10 500−14 000 cm^{-1}. From comparison with calculations, again reduced by 3000 cm^{-1}, the most likely assignment appears to be attribution of the first two peaks to vibrational structure of a transition to the 2B state and of the broader third peak to a transition to the 2A state. The asymmetrically shaped intense peak at ∼15 000 cm^{-1}, with an absorption coefficient of ∼23 500 ± 4700 M^{-1} cm^{-1}, is attributed to a transition to the 3A state. Another possible assignment would be to attribute both 2A and 3A to the most intense peak. A polarization measurement would allow the uncertainty to be removed.

As seen in Figure 12, the transitions into the 1A and 3A states correspond to electron promotions from the SOMO −1b to MOs −1a and −2a, and thus to transitions to the 1A and 2A states in the T_1-T_x spectrum. Transitions to the 2B and 3B states are attributed to electron promotions from the SOMO to MOs −2b and −3b, and accordingly are analogous to transitions to the 2B and 3B states in the T_1-T_x spectrum. The prominent transition to the 2A state of $\mathbf{1}^{-\bullet}$ is due to electron promotion from the HOMO 1a to the SOMO −1b and, therefore, is entirely analogous to the 1B transition in $\mathbf{1}^{+\bullet}$, which occurs at the same energy, and to the L_1 transition in neutral **1**, which occurs ∼8000 cm^{-1} higher (Table 7).

Figure 12 shows an additional pair of vacant orbitals in $\mathbf{1}^{-\bullet}$ that is approximately degenerate with the MOs −1a, −2a, −2b, and −3b. These are the lowest calculated Rydberg orbitals,

TABLE 6: Observed and CC2 Calculated Transitions in the Radical Cation $1^{+\bullet}$ and Radical Anion $1^{-\bullet}$ [a]

$1^{+\bullet}$ D_1^+ (1A) → D_x^+						$1^{-\bullet}$ D_1^- (1B) → D_x^-					
	obsd[b]		calcd				obsd[c]		calcd		
D_x^+	$\tilde{\nu}$ 10^3 cm^{-1}	f[d]	$\tilde{\nu}$ 10^3 cm^{-1}	f[d]	pol[e]	D_x^-	$\tilde{\nu}$ 10^3 cm^{-1}	f[d]	$\tilde{\nu}$ $10^3 cm^{-1}$	f[c]	pol[e]
1B	14.2	0.023	18.6	0.0019	*y*	1A			13.7	0.024	*y*
2B	18.5	0.25	21.6	0.67	*y*	2B	10.6	0.037	14.1	0.12	*z*
2A			21.6	0.059	*z*	2A	~13	0.05	16.7	0.31	*y*
3B			21.8	0.012	1.86	3B			17.3	0.0007	*z*
3A			22.1	0.058	*z*	3A	15.2	0.22	17.8	0.26	*y*
4B			24.8	0.014	0.13	4A	~18	0.015	25.2	0.068	*y*
4A			30.4	0.0035	*z*	4B			25.9	0.080	*z*
5B			31.1	0.12	*y*	5A			26.7	0.0010	15.7
5A			33.5	0.13	*z*	6A			28.8	0.0056	1.19
6A			34.8	0.0084	*z*	5B			28.9	0.0003	*z*
6B			35.0	0.0047	24.9	6B			29.2	0.0081	*z*
7A			36.0	0.0022	−*z*	7B			32.3	0.26	*z*
8A			36.9	0.0003	*z*						*z*
7B			37.2	0.021	*y*						*y*
8B			38.2	0.0006	3.31						3.31
9A			38.6	0.0048	*z*						*z*

[a] Vertical excitation energies of the C_2 conformer calculated at the equilibrium geometry of the ground state. State symmetry assignments are based only on calculations. [b] In DCE. [c] In THF. [d] Oscillator strength. [e] Axis of polarization (see formula **1** or Figure 2), or inclination of the transition moment from *y* in toward *x* in deg. Inclinations smaller than 0.1° were set equal to zero.

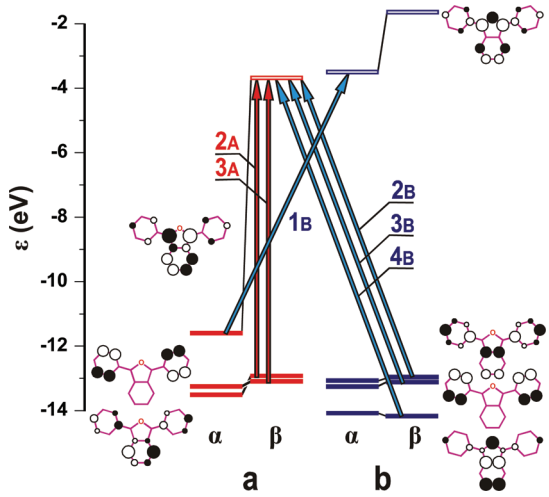

Figure 11. UHF/TZVPP orbital energies in radical cation $1^{+\bullet}$ (filled bars: occupied, empty bars: vacant). Chief contributions to $D_1 \rightarrow D_x$ excitations calculated at the CC2/TZVPP level are shown. Dashed arrows indicate that more than one electron promotion has a significant amplitude.

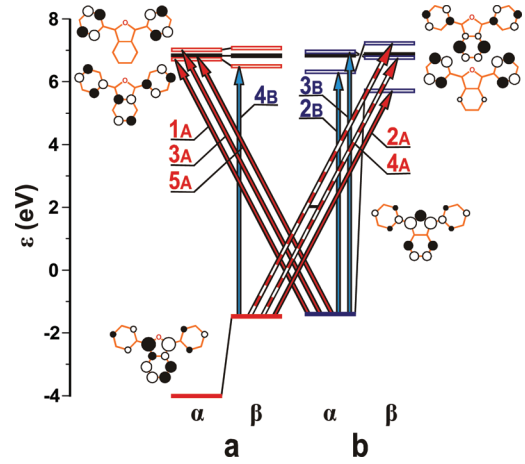

Figure 12. UHF/TZVPP orbital energies in radical anion $1^{-\bullet}$ (filled bars: occupied, empty bars: vacant, black bars: Rydberg). Chief contributions to $D_1 \rightarrow D_x$ excitations calculated at the CC2/TZVPP level are shown. Dashed arrows indicate that two electron promotions have similar amplitudes.

whose presence is not surprising in an anion. The lowest Rydberg transition is into the state 5A, but its energy is too high to appear in Figure 10.

Relations between the Spectra of 1, $1^{+\bullet}$, and $1^{-\bullet}$. Table 7 summarizes the correspondence of singly excited configurations to electron promotions that generate the singlet, triplet, and doublet electronic states observed and calculated in the various spectra of **1** and its radical ions.

Discussion

Molecular Geometry (Tables 1 and 2). There is nothing surprising about the geometry of **1** obtained from single crystal X-ray diffraction. The high degree of planarity and partial localization of double bonds in the isobenzofuran moiety in the sense of the valence bond structure **1** corresponds to expectations, with the nominally double bonds at ~1.365 Å only a little longer than an isolated C═C bond, and the nominally single bonds much longer at ~1.435 Å, but still significantly shorter than pure single bonds between sp^2 hybridized carbon atoms. The ~24° out-of-plane twist of the phenyl substituents, attributed to steric repulsions of the ortho hydrogen atoms as usual, is somewhat smaller than in biphenyl, as would be expected since the hydrogens will interfere less when one of the rings is five-membered.

The various quantum chemical methods all perform quite well but differ somewhat in their ability to render the effects of π-electron conjugation on bond lengths accurately. The experimental average difference between the nominally double and nominally single bonds is ~0.07 Å. The CASSCF(12,12) procedure yields ~0.08 Å and thus underestimates the effect of π conjugation slightly, whereas B3LYP (0.05 Å) and especially the MP2 and CC2 (0.03) methods overestimate it. When judged by the calculated twist angle of the phenyl group, which involves a balance of the effects of π conjugation and van der Waals repulsion, the CASSCF(12,12) method (~32°) overestimates the observed ~24° angle, the B3LYP procedure (~21°) underestimates it slightly, and both MP2 and CC2 reproduce it accurately. It is possible, however, that the

TABLE 7: Representation of Low-Energy Spectral Transitions in 1, $1^{+\bullet}$, and $1^{-\bullet}$ by Single Electron Promotions

MO		S_0-S_x	S_1-S_x	T_1-T_x	$D_1^+ \rightarrow D_x^+$	$D_1^- \rightarrow D_x^-$
initial	final	1A →	1B →	1B →	1A →	1B →
1a	−1b	1B			1B, 2B	2A
1b	1a				1B, 2B	
1a	−2b	2B				4A, 6A
1a	−3b	3B				4A, 6A
1a	−1a	2A				4B
1a	−2a	3A				
2a	−1b	4B, 5B				
3a	−1b	4B, 5B				
1b	−1b	4A				
2b	−1b	5A				
2a	1a		4B, 5B	4B, 5B	3A	
3a	1a		4B, 5B	4B, 5B	2A	
1b	1a		4A	4A		
2b	1a		5A, 6A	5A	3B	
3b	1a		5A, 6A	3A	4B	
−1b	−2b		2B	2B		2B
−1b	−3b		3B	3B		3B
−1b	−1a		2A	1A		1A
−1b	−2a		3A	2A		3A

experimental value is affected by crystal packing forces and would be somewhat larger in an isolated molecule, and that the poorer performance of the CASSCF(12,12) method in this instance is only apparent.

The CC2 computed geometries of the C_2 and the C_s conformers of **1** are virtually identical, and the only significant difference is the relative sign of the twist angles of the two phenyl groups.

Geometry changes upon excitation are of particular interest in the present context. The size of the molecule precluded the use of the most accurate CAS-PT2 procedure for geometry optimization and forced us to rely on the less expensive CC2 method of calculation, which can be applied for all of the species of interest here. In the companion papers[18] that deal with the covalent dimers of **1**, we use the even less expensive TD-DFT/B3LYP approach to compare the geometries of the dimers calculated in various electronic states with those of **1**.

In **1**, the lowest singlet (S_1) excitation, and even more so, the lowest triplet (T_1) excitation reduce the length of the nominally single bonds and increase the length of the nominally double bonds of the ground state, nearly equalizing the bond lengths around the perimeter of the π-conjugated isobenzofuran moiety. The difference of the vertical and the adiabatic excitation energy is 2000 cm^{-1} for S_1 and 1600 cm^{-1} for T_1. Given that both the S_1 and the T_1 excitation are of the HOMO−LUMO type, the pattern of bond length changes upon excitation fits expectations based on the nodal properties of the SCF MOs shown in Figure 6, but also more simply the perimeter MOs or Hückel MOs of isobenzofuran. A simplified description of the geometrical changes induced by S_1 or T_1 excitation is to say that it enhances the effect of π conjugation. Similar arguments account for the calculated reduction of the twist angle of the phenyl groups from 24° to 9−10°. As is apparent in Figure 6, occupancy of the HOMO does not contribute to the bond order of the exocyclic bonds, while occupancy of the LUMO does. The reduced twist angle makes the distinction between the C_2 and C_s conformers in the S_1 state rather precarious.

In the second lowest excited singlet state S_2 the calculated adiabatic excitation energy is 1600 cm^{-1} lower than the vertical excitation energy, and the phenyl groups are twisted by 22°, nearly as much as in the ground state. This is again readily understood by inspection of the MOs in Figure 6, since unlike the occupancy of the LUMO, the occupancy of LUMO+1 makes no contribution to the bond order of the exocyclic bonds.

As expected, the calculated geometry changes upon going from the ground state of **1** into its ionized states are similar to those that are predicted for electronic excitation, but less pronounced. The computed geometries of the radical cation and radical anion are fairly similar except for the striking difference in the phenyl twist angles, which can again be understood upon inspection of the MOs in Figure 6. While in $\mathbf{1}^{+\bullet}$ this angle is nearly the same as in the ground state of **1**, in $\mathbf{1}^{-\bullet}$ it is mere ∼7°, even somewhat smaller than in the excited states.

The relatively large differences in the geometries of the ground state of **1** and its excited and ionized states suggest that the internal reorganization energies for energy and charge transfer processes will be significant, making these processes less favorable, and possibly counteracting the favorable relative disposition of the S_0, T_1, and T_2 energies for singlet fission. We shall return to this issue in a subsequent paper of the series.[18]

Conformers. The calculations that suggest that in the ground state C_2 and C_s conformers coexist in comparable amounts under equilibrium conditions are undoubtedly reliable, but it is not easy to obtain direct experimental evidence for their presence since most of their properties except shape are so similar, and since their interconversion is undoubtedly fast, certainly at room temperature. The IR spectra of the conformers calculated at the B3LYP/6-311G* level were essentially identical. The calculated electronic transition energies (Table 4) are virtually identical as well. In the excited states, for which the twist angles are computed to be smaller, there may well be only one minimum in the potential energy surface and the distinction between the conformers is lost. This could account for the emission peaks being somewhat narrower than absorption peaks (Table 3).

The relatively small observed degree of alignment of **1** in stretched polyethylene was expected from the nearly equal dimensions of its molecule in the y and z directions. The exquisite sensitivity of the degree of orientation in stretched polyethylene to molecular shape allowed us to demonstrate the presence of two species, presumably the C_2 and C_s conformers, and to separate their absorption spectra in the region of the purely polarized first band. Their Franck−Condon envelopes differ to a surprising degree, and this result appears to be worth further investigation. As noted above, the existence of two conformers may be related to some of the unusual sensitivity of the photophysical properties of thin films of **1** on the mode of deposition. There are a large number of π-electron systems that are expected to exhibit similar conformational isomerisms, such as terphenyl, and little if anything is known at present about the spectral differences.

Additional information on the separate existence and properties of the two calculated isomers of **1** and similar compounds could be obtained (i) either by high-resolution fluorescence excitation spectroscopy in a supersonic jet (ii) or by a study of partial circular polarization in fluorescence excited with circularly polarized light, which should be exhibited by the chiral C_2 conformer but not the achiral C_s conformer. This may be worth pursuing in the future, but it did not appear essential for the present purposes, and in the following we assume that the spectral and photophysical properties of the two conformers are essentially identical.

Electronic Excited States. An understanding of the location and nature of singlet electronic states in **1** is essential for an understanding of the photophysics of this compound and its covalent dimers in solution and in the solid phase and thus for

the study of singlet fission. The combined knowledge of transition polarizations and MCD *B* terms in S_0-S_x spectra and the additional knowledge of the S_1-S_x spectrum permitted a detailed interpretation of the electronic structure of the excited states. It is particularly satisfying that the CC2 and singly excited PPP computations account for the observed spectra well, providing credence to the detailed description of the excited states in terms of the MOs involved in the excitations. It also is gratifying that some of the spectral features, especially the MCD signs of the L_1, L_2, and most likely even the B_1 transitions, can be interpreted without any calculation in terms of the simple perimeter model.[71,72]

The systematic error of the CC2 method, which underestimates all excitation energies by about 3000 cm^{-1}, is undoubtedly due to a differentially better description of the initial state than the higher energy final state. It is unfortunate but does not destroy the utility of the method for spectral interpretations. For π-electron systems of this size, better methods of calculation are not practical when excited state geometries need to be optimized. Elsewhere,[73] we will present a comparison of the performance of a series of methods for vertical excitations. The results do not change the CC2-based interpretations presented here.

It is striking that the extremely simple singly excited PPP method based on standard parameters yields results that are so similar to the CC2 results in terms of the description of the nature of the excitations, and superior in terms of calculated energies, which require no empirical adjustment. Of course, a simple nearly planar π-electron heterocycle such as **1** represents a particularly favorable case for the PPP method, and the CC2 procedure is much more widely applicable.

The excitation energies, S_0-S_1 observed at ~24 300 cm^{-1} (vertical) and nearly independent of solvent choice, S_0-T_1 observed at ~11 900 cm^{-1} (adiabatic), and S_0-T_2 calculated at 28 500 cm^{-1} (vertical) and estimated at 25 500 cm^{-1} after an empirical correction, satisfy the conditions $E(S_1)$, $E(T_2) \geq 2\,E(T_1)$, considered optimal for singlet fission. The slightly lower value of ~11 400 cm^{-1} obtained for $E(T_1)$ presently by EELS is probably due to a small red shift upon going from solution to the solid state. The somewhat higher value of 12 900 ± 400 cm^{-1} obtained from electroluminescence[24] is considered less reliable.

The solution photophysics is extremely simple, as fluorescence from S_1 is the only observed fate of the singlet excited molecule in the range of excitation energies examined. The observed fluorescence rate constant of ~0.15 ns^{-1} clearly is at least 2 and probably 3 orders of magnitude larger than the rate constant of any possibly competing process, such as intersystem crossing into the T_1 state. Along with the favorable disposition of the energy levels, this makes **1** an excellent candidate for singlet fission studies. It helps that the T_1 state exhibits a characteristic and intense absorption peak in a favorable spectral region and is long-lived. Its first-order decay lifetime of ~0.2 ms in the high dilution limit is attributed to intersystem crossing to the ground state.

The fluorescence excitation curve follows the absorption curve faithfully up to 37 000 cm^{-1}. Its sudden drop-off at this energy, however, suggests the onset of a nonradiative decay channel, perhaps due to a hot excited state photochemical transformation, such as closure of the 1,3-butadiene moiety in the five-membered ring to a cyclobutene moiety, most likely rapidly reversed thermally upon relaxation in the ground S_0 state.

Spectra of Radical Ions. The spectra of $\mathbf{1}^{+\bullet}$ and $\mathbf{1}^{-\bullet}$ will be useful for the interpretation of the photophysics of covalent dimers of **1** in polar solvents. The agreement of CC2 calculated and observed spectra has permitted state assignments and interpretation of transitions in terms of orbitals involved. In addition to the 1B excitation that corresponds to the HOMO−LUMO transition in neutral **1**, transitions in the radical cation involve promotions of an electron into the SOMO. Comparison of Figures 11 and 12 with Figures 7 and 9 shows that they are entirely analogous to the higher energy half of the T_1-T_x or S_1-S_x transitions. Since configuration interaction plays a minor role in the description of the low-energy states of $\mathbf{1}^{+\bullet}$ (Figure 11), it should be possible to obtain a qualitative estimate of the energies required for promotion to the SOMO from the knowledge of the energies of the occupied MOs of **1**, using arguments based on Koopmans' theorem.[74] For best results, the orbital energies should be evaluated at the equilibrium geometry of $\mathbf{1}^{+\bullet}$, but even using MO energies obtained at the equilibrium geometry of **1** the comparison is fairly favorable for the lowest few excitations into the SOMO. In units of 10^3 cm^{-1}, for the 2B, 2A, 3B, and 3A excitations, the CC2 excitation energies listed in Table 6 are 21.6, 21.6, 21.8, and 22.1 and those obtained from MO energy differences are 22.4, 23.7, 23.8, and 24.8, respectively.

Similarly, in addition to the 2A excitation that corresponds to the HOMO−LUMO transition in neutral **1**, transitions in the radical anion mostly involve promotions of an electron from the SOMO and are entirely analogous to the lower energy half of the T_1-T_x or S_1-S_x transitions. The HOMO−LUMO type transition, present in the spectra of neutral **1** and its radical ions, is naturally absent in the T_1-T_x spectrum. It should be present in the S_1-S_x spectrum, yielding a closed-shell doubly excited electron configuration, but apparently occurs at energies higher than those examined presently.

The existence of qualitative relations between the spectra of excited states of an excited neutral species and the spectra of its radical ions (Table 7) is nothing new, but it is not often that one can see these relations illustrated with ab initio calculations on a relatively complex π electron system.

Conclusions

The spectroscopic and photophysical properties of **1** have been found to be suitable for a detailed examination of singlet fission in its covalent dimers, oligomers, polymers, aggregates, and nanocrystals. A detailed understanding of its structure and electronic states has been obtained, including transition polarization, magnetic circular dichroism, and the spectra of its radical ions, and the photophysics of its covalent dimers can now be tackled. Since its two conformers orient to a different degree in stretched polyethylene, it has been possible to separate their spectra in the region of the purely polarized first absorption band.

Acknowledgment. We acknowledge support from the U.S. Department of Energy, Office of Energy Efficiency and Renewable Energy, Photovoltaics Program (A.F.S., M.B.S., D.P., I.P., A.A., M.K.M., X.C., D.E.D., M.A.R., and J.M., XAT-5-33636-01 and DE-FG36-08GO18017), U.S. Department of Energy, Office of Basic Energy Sciences, Division of Chemical Sciences, Biosciences, and Geosciences (J.C.J. and A.J.N., DE-AC36-08GO28308; P.S. and J.R.M., DE-AC02-98-CH10886), and the NSF (OISE-0532040), and the KONTAKT project of the Ministry of Education, Youth, and Sport of the Czech Republic (J.Č. and Z.H., ME09114).

Supporting Information Available: X-ray diffraction structure of **1**, available as a CIF file, Figure S1 of polarized spectra

of **1**, and complete ref 46. This material is available free of charge via the Internet at http://pubs.acs.org.

References and Notes

(1) Nozik, A. J.; Ellingson, R. J.; Micic, O. I.; Blackburn, J. L.; Yu, P.; Murphy, J. E.; Beard, M. C.; Rumbles, G. *Proceedings of the 27th DOE Solar Photochemistry Research Conference, June 6−9, 2004, Airline Conference Center, Warrenton, VA*; 2004; pp 63−66. Available on line: http://www.sc.doe.gov/ BES/chm/Publications/Contractors%20Meetings/27th_DOE_Solar_Photochemistry_crop.pdf.

(2) Michl, J.; Chen, X.; Rana, G.; Popović, D. B.; Downing, J.; Nozik, A. J.; Johnson, J. C.; Ratner, M. A.; Paci, I. *Book of Abstracts, DOE Solar Program Review Meetings, October 24−28, 2004, Denver, CO*; U.S. Department of Energy: Washington, DC, 2004; p 5.

(3) Johnson, J. C.; Nozik, A. J.; Paci, I.; Ratner, M. A.; Popović, D. B.; David, D. E.; Chen, X.; Rana, G.; Michl, J. *Book of Abstracts, International Chemical Congress of Pacific Basin Societies, Honolulu, HI, December 15−20, 2005*; Scholar One, Inc.: Charlottesville, VA, 2005; abstract 1597.

(4) Paci, I.; Johnson, J. C.; Chen, X.; Rana, G.; Popović, D.; David, D. E.; Nozik, A. J.; Ratner, M. A.; Michl, J. *J. Am. Chem. Soc.* **2006**, *128*, 16546–16553.

(5) Singh, S.; Jones, W. J.; Siebrand, W.; Stoicheff, B. P.; Schneider, W. G. *J. Chem. Phys.* **1965**, *42*, 330–342.

(6) Swenberg, C. E.; Geacintov, N. E. In *Organic Molecular Photophysics*, Birks, J. B., Ed.; Wiley: New York, 1973; Vol. 1, pp 489−564.

(7) Hanna, M. C.; Nozik, A. J. *J. Appl. Phys.* **2006**, *100*, 074510−074518.

(8) Shockley, W.; Queisser, H. J. *J. Appl. Phys.* **1961**, *32*, 510–519.

(9) Nozik, A. J. *Physica E* **2002**, *14*, 115–120.

(10) Ellingson, R. J.; Beard, M. C.; Johnson, J. C.; Yu, P.; Micic, O. I.; Nozik, A. J.; Shabaev, A.; Efros, A. L. *Nano Lett.* **2005**, *5*, 865–871.

(11) Schaller, R. D.; Klimov, V. I. *Phys. Rev. Lett.* **2004**, *92*, 186601−1186601−4.

(12) Nozik, A. J. *Chem. Phys. Lett.* **2008**, *457*, 3–11.

(13) Müller, A. M.; Avlasevich, Y. A.; Müllen, K.; Bardeen, C. J. *Chem. Phys. Lett.* **2006**, *421*, 518–522.

(14) Müller, A. M.; Avlasevich, Y. A.; Schuller, W. W.; Müllen, K.; Bardeen, C. J. *J. Am. Chem. Soc.* **2007**, *129*, 14240–14250.

(15) Michl, J.; Nozik, A. J.; Chen, X.; Johnson, J. C.; Rana, G.; Akdag, A.; Schwerin, A. F. In *Organic Photovoltaics* VIII; Kafafi, Z. H., Lane, P. A., Eds.; Proceedings of SPIE, Vol. 6656; SPIE: Bellingham, WA, 2007; pp 66560E1−66560E9.

(16) Greyson, E. C.; Stepp, B. R.; Chen, X.; Schwerin, A. F.; Paci, I.; Smith, M. B.; Akdag, A.; Johnson, J. C.; Nozik, A. J.; Michl, J.; Ratner, M. A. *J. Phys. Chem. B*, in press.

(17) Greyson, E. C.; Vura-Weis, J.; Michl, J.; Ratner, M. A. *J. Phys. Chem. B.*, in press.

(18) Johnson, J. C.; Akdag, A.; Chen, X.; Smith, M. B.; Schwerin, A. F.; Paci, I.; Nozik, A. J.; Ratner, M. A.; Michl, J. Unpublished results.

(19) Johnson, J. C.; Smith, M. B.; Akdag, A.; Nozik, A. J.; Michl, J., Unpublished results.

(20) Marciniak, H.; Fiebig, M.; Huth, M.; Schiefer, S.; Nickel, B.; Selmaier, F.; Lochbrunner, S. *Phys. Rev. Lett.* **2007**, *99*, 176402−1-4.

(21) Thorsmølle, V. K.; Averitt, R. D.; Demsar, J.; Smith, D. L.; Tretiak, S.; Martin, R. L.; Chi, X.; Crone, B. K.; Ramirez, A. P.; Taylor, A. J. *Phys. Rev. Lett.* **2009**, *102*, 017401−1-4.

(22) Herkstroeter, W. G.; Merkel, P. B. *J. Photochem.* **1981**, *16*, 331–341.

(23) Howard, J. A.; Mendenhall, G. D. *Can. J. Chem.* **1975**, *53*, 2199–2201.

(24) Ziebig, R.; Pragst, F. *Z. Phys. Chem. (Leipzig)* **1979**, *260*, 795–803.

(25) Murray, E. C.; Keller, R. N. *J. Org. Chem.* **1969**, *34*, 2234–2235.

(26) Michl, J.; Thulstrup, E. W. *Spectroscopy with Polarized Light. Solute Alignment by Photoselection, in Liquid Crystals, Polymers, and Membranes*, 2nd ed.; VCH Publishers: Deerfield Beach, FL, 1995; (a) eq 1.24, p 28; (b) eq 1.130, p 66; (c) p 156; (d) eq 7.125, p 320; (e) pp 232ff; (f) p 135; (g) pp 230 and 404; (h) pp 195ff.

(27) Fischer, M.; Georges, J. *Chem. Phys. Lett.* **1996**, *260*, 115–118.

(28) Eaton, D. F. *Pure Appl. Chem.* **1988**, *60*, 1107–1114.

(29) David, D. E.; Popović, D. B.; Antic, D.; Michl, J. *J. Chem. Phys.* **2004**, *121*, 10542–10550.

(30) Wishart, J. F. In *Radiation Chemistry: Present Status and Future Trends*; Jonah, C. D., Rao, B. S. M., Eds.; Elsevier Science: Amsterdam, 2001; Vol. 87, pp 21−35.

(31) Wishart, J. F.; Cook, A. R.; Miller, J. R. *Rev. Sci. Instrum.* **2004**, *75*, 4359–4366.

(32) Miller, J. R.; Penfield, K.; Johnson, M.; Closs, G.; Green, N. In *Photochemistry and Radiation Chemistry. Complementary Methods for the Study of Electron Transfer*; Wishart, J. F., Nocera, D. G., Eds.; American Chemical Society: Washington. DC, 1998; Vol. 254, pp 161−176.

(33) Takeda, N.; Asaoka, S.; Miller, J. R. *J. Am. Chem. Soc.* **2006**, *128*, 16073–16082.

(34) Allen, A. O. *Natl. Stand. Ref. Data Ser.* **1976**, *57*, 16–41.

(35) Baxendale, J. H.; Beaumond, D.; Rodgers, M. A. J. *Trans. Faraday Soc.* **1970**, *66*, 1996–2003.

(36) Dodelet, J. P.; Freeman, G. R. *Can. J. Chem.* **1975**, *53*, 1263–1274.

(37) Asaoka, S.; Takeda, N.; Iyoda, T.; Cook, A. R.; Miller, J. R. *J. Am. Chem. Soc.* **2008**, *130*, 11912–11920.

(38) De Waele, V.; Sorgues, S.; Pernot, P.; Marignier, J. L.; Monard, H.; Larbre, J. P.; Mostafavi, M. *Chem. Phys. Lett.* **2006**, *423*, 30–34.

(39) *Bruker SAINT*; Bruker AXS Inc.: Madison, WI, 2001.

(40) *Bruker XPREP*; Bruker AXS Inc.: Madison, WI, 2004.

(41) Sheldrick G. M. *SADABS*; University of Göttingen: Göttingen, Germany, 2004.

(42) Sheldrick G. M. *SHELXTL*, Version 6; Bruker AXS Inc.: Madison, WI, 2001.

(43) Pariser, R.; Parr, R. G. *J. Chem. Phys.* **1953**, *21*, 466−471, 767−776.

(44) Pople, J. A. *Trans. Faraday Soc.* **1953**, *49*, 1375–1385.

(45) Castellan, A,; Michl, J. *J. Am. Chem. Soc.* **1978**, *100*, 6824–6827, and references therein.

(46) Frisch, M. J. *Gaussian 98*, revision A.9; Gaussian, Inc.: Pittsburgh, PA, 1998.

(47) Eichkorn, K.; Treutler, O.; Öhm, H.; Häser, M.; Ahlrichs, R. *Chem. Phys. Lett.* **1995**, *242*, 652−660; Erratum. *Chem. Phys. Lett.* **1995**, *242*, 283.

(48) Treutler, O.; Ahlrichs, R. *J. Chem. Phys.* **1995**, *102*, 346–354.

(49) Eichkorn, K.; Weigend, F.; Treutler, O.; Ahlrichs, R. *Theor. Chem. Acc.* **1997**, *97*, 119–124.

(50) Becke, A. D. *Phys. Rev. A* **1988**, *38*, 3098–3100.

(51) Lee, C. T.; Yang, W. T.; Parr, R. G. *Phys. Rev. B* **1988**, *37*, 785–789.

(52) Becke, A. D. *J. Chem. Phys.* **1993**, *98*, 5648–5652.

(53) Christiansen, O.; Koch, H.; Jørgensen, P. *Chem. Phys. Lett.* **1995**, *243*, 409–418.

(54) Hättig, C.; Weigend, F. *J. Chem. Phys.* **2000**, *113*, 5154–5161.

(55) Hättig, C. *J. Chem. Phys.* **2003**, *118*, 7751–7761.

(56) Weigend, F.; Häser, M.; Patzelt, H.; Ahlrichs, R. *Chem. Phys. Lett.* **1998**, *294*, 143–152.

(57) Weigend, F.; Häser, M. *Theor. Chem. Acc.* **1997**, *97*, 331–340.

(58) Ahlrichs, R.; Bär, M.; Häser, M.; Horn, H.; Kölmel, C. *Chem. Phys. Lett.* **1989**, *162*, 165–169.

(59) Pierloot, K.; Dumez, B.; Widmark, P.-O.; Roos, B. O. *Theor. Chim. Acta* **1995**, *90*, 87–114.

(60) Karlström, G.; Lindh, R.; Malmqvist, P.-Å.; Roos, B. O.; Ryde, U.; Veryazov, V.; Widmark, P.-O.; Cossi, M.; Schimmelpfennig, B.; Neogrady, P.; Seijo, L. *Comput. Mater. Sci.* **2003**, *28*, 222–239.

(61) Hättig, C.; Hald, K. *Phys. Chem. Chem. Phys.* **2002**, *4*, 2111–2118.

(62) Köhn, A.; Hättig, C. *J. Chem. Phys.* **2003**, *119*, 5021–5036.

(63) Hättig, C.; Köhn, A. *J. Chem. Phys.* **2002**, *117*, 6939–6951.

(64) Hättig, C.; Köhn, A.; Hald, K. *J. Chem. Phys.* **2002**, *116* (6), 5401–5410.

(65) Albrecht, A. C. *J. Mol. Spectrosc.* **1961**, *6*, 84–108.

(66) Radziszewski, J. G.; Michl, J. *J. Am. Chem. Soc.* **1986**, *108*, 3289–3297.

(67) Thulstrup, E. W.; Michl, J. *J. Am. Chem. Soc.* **1982**, *104*, 5594–5604.

(68) Michl, J.; Thulstrup, E. W. *Acc. Chem. Res.* **1987**, *20*, 192–199.

(69) Platt, J. R. *J. Chem. Phys.* **1949**, *17*, 484–495.

(70) Moffitt, W. *J. Chem. Phys.* **1954**, 320−333, 1820−1829.

(71) Michl, J. *Tetrahedron* **1984**, *40*, 3845–3934.

(72) Michl, J. *J. Am. Chem. Soc.* **1978**, *100*, 6801−6811, 6812−6818, 6819−6827.

(73) Havlas, Z.; Michl, J. Unpublished results.

(74) Nelsen, S. F.; Weaver, M. N.; Yamazaki, D.; Komatsu, K.; Rathore, R.; Bally, T. *J. Phys. Chem. A* **2007**, *111*, 1667–1676.

JP907401T